RADC-TR-77-232
Technical Report
July 1977

TURBULENCE ENVIRONMENT CHARACTERIZATION

Avco Everett Research Laboratory, Inc.

Sponsored by
Defense Advanced Research Projects Agency (DoD)
ARPA Order No. 2646

Approved for public release; distribution unlimited.

The views and conclusions contained in this document are those of the authors and should not be interpreted as necessarily representing the official policies, either expressed or implied, of the Defense Advanced Research Projects Agency or the U. S. Government.

ROME AIR DEVELOPMENT CENTER
Air Force Systems Command
Griffiss Air Force Base, New York 13441

This report has been reviewed by the RADC Information Office (OI) and is releasable to the National Technical Information Service (NTIS). At NTIS it will be releasable to the general public, including foreign nations.

This report has been reviewed and is approved for publication.

APPROVED: Donald W. Hanson

DONALD W. HANSON
Project Engineer

If your address has changed or if you wish to be removed from the RADC mailing list, or if the addressee is no longer employed by your organization, please notify RADC (DAP) Griffiss AFB NY 13441. This will assist us in maintaining a current mailing list.

Do not return this copy. Retain or destroy.

TURBULENCE ENVIRONMENT CHARACTERIZATION

M. G. Miller
P. L. Zieske
A. J. Sofia
R. J. Pepe

Contractor: Avco Everett Research Laboratory, Inc.
Contract Number: F30602-76-C-0054
Effective Date of Contract: 15 October 1976
Contract Expiration Date: 15 April 1978
Short Title of Work: Turbulence Environment Characterization
Program Code Number: 7E20
Period of Work Covered: Oct 76 - Mar 77

Principal Investigator: Dr. M. G. Miller
Phone: 617 389-3000, ext. 528
Project Engineer: Donald W. Hanson
Phone: 315 330-3144

This research was supported by the Defense Advanced Research Projects Agency of the Department of Defense and was monitored by Donald W. Hanson (OCSE), Griffiss AFB NY 13441 under Contract F30602-76-C-0054.

UNCLASSIFIED

SECURITY CLASSIFICATION OF THIS PAGE (When Data Entered)

(18) (19) REPORT DOCUMENTATION PAGE		READ INSTRUCTIONS BEFORE COMPLETING FORM
1. REPORT NUMBER RADC-TR-77-232	2. GOVT ACCESSION NO.	3. RECIPIENT'S CATALOG NUMBER
(6) 4. TITLE (and Subtitle) TURBULENCE ENVIRONMENT CHARACTERIZATION		(9) 5. TYPE OF REPORT & PERIOD COVERED Interim Report 15 Sep 76 - 15 Mar 77
		6. PERFORMING ORG. REPORT NUMBER N/A
(10) 7. AUTHOR(s) M. G. Miller, R. J. Pepe P. L. Zieske A. J. Sofia		(15) 8. CONTRACT OR GRANT NUMBER(s) F30602-76-C-0054 ARPA Order-2646
9. PERFORMING ORGANIZATION NAME AND ADDRESS Avco Everett Research Laboratory, Inc. 2385 Revere Beach Parkway Everett MA 02149		10. PROGRAM ELEMENT, PROJECT, TASK AREA & WORK UNIT NUMBERS 62301E 26460115
11. CONTROLLING OFFICE NAME AND ADDRESS Defense Advanced Research Projects Agency 1400 Wilson Blvd Arlington VA 22209		(11) 12. REPORT DATE July 1977 13. NUMBER OF PAGES 68 (12) 67 P.
14. MONITORING AGENCY NAME & ADDRESS (if different from Controlling Office) Rome Air Development Center (OCSE) Griffiss AFB NY 13441	(16) 2646 (17) 01	15. SECURITY CLASS. (of this report) UNCLASSIFIED 15a. DECLASSIFICATION/DOWNGRADING SCHEDULE N/A

16. DISTRIBUTION STATEMENT (of this Report)

Approved for public release, distribution unlimited.

17. DISTRIBUTION STATEMENT (of the abstract entered in Block 20, if different from Report)

Same

18. SUPPLEMENTARY NOTES

RADC Project Engineer:
Donald W. Hanson (OCSE)

19. KEY WORDS (Continue on reverse side if necessary and identify by block number)

Turbulence
Seeing
Atmospheric Optics
Scintillation
DARPA

20. ABSTRACT (Continue on reverse side if necessary and identify by block number)

This report contains discussions of a variety of activities and results relative to the characterization of atmospheric turbulence and its effects on optical propagation at the AMOS Observatory on Maui, Hawaii. Work carried out during this reporting period has included: (1) deployment and testing of new and/or modified instrumentation; (2) routine data collection; (3) special experiments for instrument characterization and calibration, and, (4) theoretical and statistical analysis of the resulting data. (cont'd)

DD FORM 1 JAN 73 1473 EDITION OF 1 NOV 65 IS OBSOLETE

UNCLASSIFIED

SECURITY CLASSIFICATION OF THIS PAGE (When Data Entered)

048 450

The acoustic sounder was returned to the site after modification in November 1976 and is now operational, except for final calibration against the microthermal probes. The RTAM underwent a second series of field tests and has been used to collect simultaneous data with the Seeing Monitor. Real time, analog processing electronics for RTAM have been designed and fabricated.

The results of routine data collection during this period yields a mean of 10.7 cm and a range of (3.6-16.7) cm for the atmospheric correlation scale (r_o). Aperture averaged (36 cm) log-amplitude variances have a mean of 5.9×10^{-4} and a range of $(1.8\text{-}14) \times 10^{-4}$. Upper atmospheric profiles are similar to those previously reported. Apparent atmospheric non-stationarity has continued to invalidate approximately 40% of the profiles.

A series of noise evaluation tests with the Seeing Monitor have shown a performance consistent with expectation but with a noise contribution to the voltage variance higher than that predicted by theory. An operational threshold of visual magnitude + 4 has been set for the collection of reliable data with this device. Comparative Speckle Interferometer/Seeing Monitor data shows significant differences. The reason for the disagreement is unknown.

An analysis of the statistical properties of the values of C_n^2 obtained from the Star Sensor yields rough agreement with the Hufnagel wind correlated model; however, the data does not support the existence of as strong a tropopause layer as does the model.

PREFACE

This report is submitted in compliance with the requirements of Contract F30602-76-C-0054 and covers work carried out during the period 15 September 1976 to 15 March 1977. Earlier work is reported in RADC-TR-77-70 (March 1977). Related work under a previous contract (F30602-75-C-0012) is reported in RADC-TR-75-185 (July 1975) and RADC-TR-76-189 (June 1976).

We would like to thank the staff of the AMOS Observatory for assistance in collecting the data. We also acknowledge the assistance and support of D. Tarazano of RADC and A. MacGovern and J. LeFebvre of Itek, Inc.

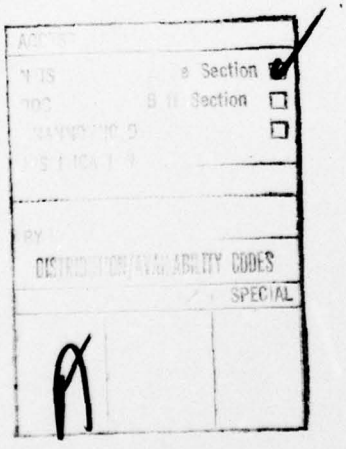

TABLE OF CONTENTS

LIST OF ILLUSTRATIONS

LIST OF TABLES

1.0 INTRODUCTION

1.1 BACKGROUND AND OBJECTIVES

This report describes recent activities and results relative to the characterization of atmospheric turbulence and its effects on the propagation of electromagnetic radiation at the ARPA Maui Optical Station (AMOS) atop Haleakala on the Island of Maui, Hawaii. An extensive set of instrumentation has been deployed at the site over the last several years which measures several properties of the turbulent field as well as its effects on optical propagation. The primary objective of this work is to establish a comprehensive data base which can be used to verify theory and provide input to optical system design studies and specifications. Discussions of the experimental systems, earlier results and other relevant information are given in References 1, 2 and 3.

During this reporting period several activities have been carried out. These include: (1) deployment and testing of new and/or modified instrumentation; (2) routine data collection; (3) special experiments for instrument characterization and calibration, and (4) theoretical and statistical analysis of the resulting data. The program status, accomplishments and the most significant results and conclusions are given below. Section 2.0 summarizes the experimental operations and instrumentation status and includes discussions of the modified acoustic sounder and Real Time Atmospheric Measurement (RTAM) System. The experimental data and its analysis is summarized in Section 3.0. Included are discussions of the routine Seeing Monitor and Star Sensor data, Seeing Monitor noise evaluation data, Seeing Monitor/Speckle Interferometer comparative data, a statistical analysis of Star Sensor turbulent profile data and RTAM data.

---

(1) M. G. Miller and P. F. Kellen, Turbulence Characterization and Control, Interim Technical Report, Contract F30602-75-C-0012 (Avco Everett Research Laboratory, Inc.), Rome Air Development Center Technical Report #RADC-TR-75-185 (July 1975).

(2) M. G. Miller, P. L. Zieske and G. Dryden, Turbulence Characterization and Control, Final Technical Report, Contract F30602-75-C-0012 (Avco Everett Research Laboratory, Inc.), Rome Air Development Center Technical Report #RADC-TR-76-189 (June 1976).

(3) M. G. Miller and P. L. Zieske, Turbulence Environment Characterization, Interim Technical Report, Contract F30602-76-C-0054 (Avco Everett Research Laboratory, Inc.), Rome Air Development Center Technical Report #RADC-TR-77-70 (March 1977).

1.2 PROGRAM STATUS AND ACCOMPLISHMENTS

As of the date of this report, the status of the instrumentation is as follows.

- The Seeing Monitor, Star Sensor and PDP-8 data processing system have continued to operate reliably. However, the Star Sensor has been removed from the Teal Amber dome because of the requirements of other programs.
- Microthermal probe failures due to weather continues to be a problem.
- The dew point sensor failed and was returned to the manufacturer for repair. The other routine meteorological instrumentation is performing reliably.
- The acoustic sounder was returned to the site and, except for final calibration, is operational.
- The RTAM has been delivered to AMOS.

Significant accomplishments include:

- Continued routine data collection with the Seeing Monitor and Star Sensor.
- The completion of Seeing Monitor noise evaluation experiments and the reduction of comparative Seeing Monitor/Speckle Interferometer data.
- Successful acoustic sounder operation and data reduction.
- Simultaneous data collection with the RTAM and Seeing Monitor.
- The design and fabrication of RTAM analog processing electronics.

1.3 RESULTS AND CONCLUSIONS

Data was collected with the Seeing Monitor on ten occasions. The results yield the following information.

- A mean value of r_o at 5000 Å of 10.7 cm with a range of (3.6 to 16.7) cm. These results are not significantly different from previously reported data.
- Simulated magnitude sequences yield an SM performance consistent with expectation. However, the noise levels appear to be higher than theoretically predicted.
- An operational threshold of visual magnitude +4 has been set for the collection of reliable data with the SM.

The reduction of several nights of comparative Seeing Monitor/ Speckle Interferometer data yields the following information.

- There are significant differences between the two measurements. The SI value for r_o is generally higher, but considerable dispersion exist in the results.
- The reason for this disagreement is unknown.

Data was collected with the Star Sensor on eight occasions. The results yield the following information.

- Upper atmospheric profiles similar to previously reported results.
- Apparent atmospheric non-stationarity continues to invalidate approximately 40% of the profiles.
- Aperture averaged twenty minute log-amplitude variances with a mean of 5.88×10^{-4} and a range of $(1.8 - 14.1) \times 10^{-4}$. This data is very consistent with previously reported results.

The analysis of average properties of Star Sensor profiles yields the following information.

- The data is consistent with the Hufnagel wind correlated model. However, the best fit of the model to the data results in a rather low value (12.5 m/s) for the average wind speed.
- The data (on the average) is not consistent with a strong tropopause turbulence layer.

Field operations with the modified RTAM yield the following information.

- A considerable improvement in otpical performance, in particular, the instrumental field of view.
- A sensitivity which should be sufficient to allow simultaneous operations with the Seeing Monitor with the objective of obtaining comparative r_o estimates.

2.0 EXPERIMENTAL OPERATIONS AND INSTRUMENTATION

2.1 OPERATIONS

During this reporting period data collection operations were not as intensive as during the previous contract period. Several reasons contributing to this were: (1) higher priority activities at AMOS; (2) a two operations per week schedule; (3) receiving and acceptance testing of other systems; and (4) special systems testing. Twenty-five data missions were scheduled. Data was not obtained on seven occasions because of weather, equipment problems or priority conflicts. The remaining 18 missions obtained data as indicated in Table 1.

In the November time period extensive training missions were carried out on the reconditioned acoustic sounder. Because the system was not calibrated at that time, the resulting data has not been included in this report.

Acceptance testing of the Real Time Atmospheric Measurement (RTAM) system occurred in January and required three days of bench checkout and two nights of telescope time. After acceptance, familiarization tests, utilizing AMOS personnel only, were conducted. The RTAM and Seeing Monitor were then mounted and aligned on the Atmospheric Seeing Package (ASP) with a common boresight and remounted on the 1.6 m telescope in order to obtain simultaneous RTAM/SM data for latter processing. Four nights were scheduled and reducible data recorded on two of them. The data reduction portion of this task has not yet been completed.

Other activities, relative to special systems testing and upgrading, were also carried out. One of these was a series of short cycle time, variable object magnitude, data collection with the Seeing Monitor. The objective of these operations was to experimentally evaluate the noise characteristics of this device. Another was the operational verification of a number of modifications to the Star Sensor software.

2.2 INSTRUMENTATION

A number of modifications and additions to existing instrumentation were made during this reporting period. The more important ones are as follows.

In order to evaluate noise characteristics of the Seeing Monitor, a filter wheel was designed, fabricated and installed in the optical train of the ASP. The wheel is a simple, five hole, gear driven disk containing glass neutral density filters of value 0.5, 1.0, 2.0 and 3.0. The fifth hole is open and provided a completely unvignetted and unattenuated beam to the sensors. Any of the five positions can be remotely selected from the Atmospherics Control Room.

TABLE 1. AMOS ATMOSPHERICS MEASUREMENTS SUMMARY

DATA	RTAM	AS	SS	SM	ARN
DATE					
22 Sep 76			X		760922
24			X	X	760924
27 Oct 76			X	X	761027
28			X	X	761028
29			X	X	761029
09 Dec 76				X[2]	761209
10		X	X	X[2]	761210
12 Jan 77		X[1]	X	X[2]	770112
13		X[1]	X	X[2]	770113
26	X[3]				770126
28	X[3]				770128
31	X[4]				770131
01 Feb 77	X[4]				770201
02	X[4]				770202
03	X[4]				770203
14	X[5]*			X[5]*	770214
16	X[5]			X[5]	770216
17	X[5]			X[5]	770217

AS = Acoustic Sounder
SS = Star Sensor
SM = Seeing Monitor
ARN = Atmospheric Run No.
RTAM = Realtime Atmospheric Measurement System

1 = Training Only
2 = No Tests
3 = Acceptance Tests
4 = Familiarization Tests
5 = RTAM/SM Simultaneous Tests
* = No Reducible Data Recorded

A high speed reader/puncher (PC-04) was installed in the PDP-8I computing system to provide high speed loading of the Maui Means and Variance Program and the Mk 5.0 sounder program. In addition to the time saving (fifteen to one time compression) a significant increase in accuracy is obtained as a result of bypassing the ASR 33 low speed tape reader which, because of its age, is difficult to keep in adjustment. The PC-04 unit is shown in Figure 1.

Another instrumentation change effected during this period was the design and fabrication of a beam splitting system for the ASP so that both the Seeing Monitor and RTAM system could share the 1.6 m telescope beam. This was accomplished by use of a specially coated cube beam splitter and auxillary optics. Special adjustable fixturing was made to hold mirrors and the splitter in such a manner that 28% of the light was directed to the Seeing Monitor, 64% to the RTAM and the remaining 8% to the boresight camera. Because one of the components of the split beam was out of plane with the RTAM entrance aperture, an additional folding flat and angle adjustable mounts were required to align the beam with the RTAM.

Early in March the Star Sensor, Celestron telescope and telescope pier were demounted from the Teal Amber dome. This was done so that certain Teal Amber measurement activities and repair tasks could be accomplished. The repair tasks are still pending but are expected to be finished in early summer. In an attempt to provide local time and a data summary, software changes were made to the NOVA 2/10 program. By using a simple analog timing device interfaced to the NOVA's A/D Converter individual star sensor summaries can be time tagged. This timing subsystem will be tested as soon as the star sensor system is reinstalled in the Teal Amber dome and normal operations resumed.

2.3 ACOUSTIC SOUNDER

The acoustic sounder was returned to the site in early November and installed and checkout jointly by AMOS and RADC personnel. The transducer was upgraded from a 40 W unit to the 100 W model. Preamplifier gain was reduced to 90 dB, receiver gain was reduced to a net zero dB from 16 dB and filter gain was kept at 46 dB for a net system gain (after losses) of 109 dB. A new feature of the acoustic sounder system is the Mk 5.0 version of the sounder reduction program. This software, while still being a 20 level reduction program, allows for the continuous input of ambient temperature, dew point and barometric pressure. This capability will significantly improve the accuracy of the C_n^2 profile data produced during periods of rapid change, such as sunset and sunrise transition periods, wind shifts and frontal passage. It is hoped that the addition of the 100 W transducer will offset the loss in system performance due to lower system gain and that a 300 m ceiling will still be attainable. Once the sounder apparatus was reinstalled at the site, extensive system testing (mostly daytime) was carried out in conjunction with the Bell & Howell tape recorder. These tests confirmed that the reconditioned system was performing in a normal manner.

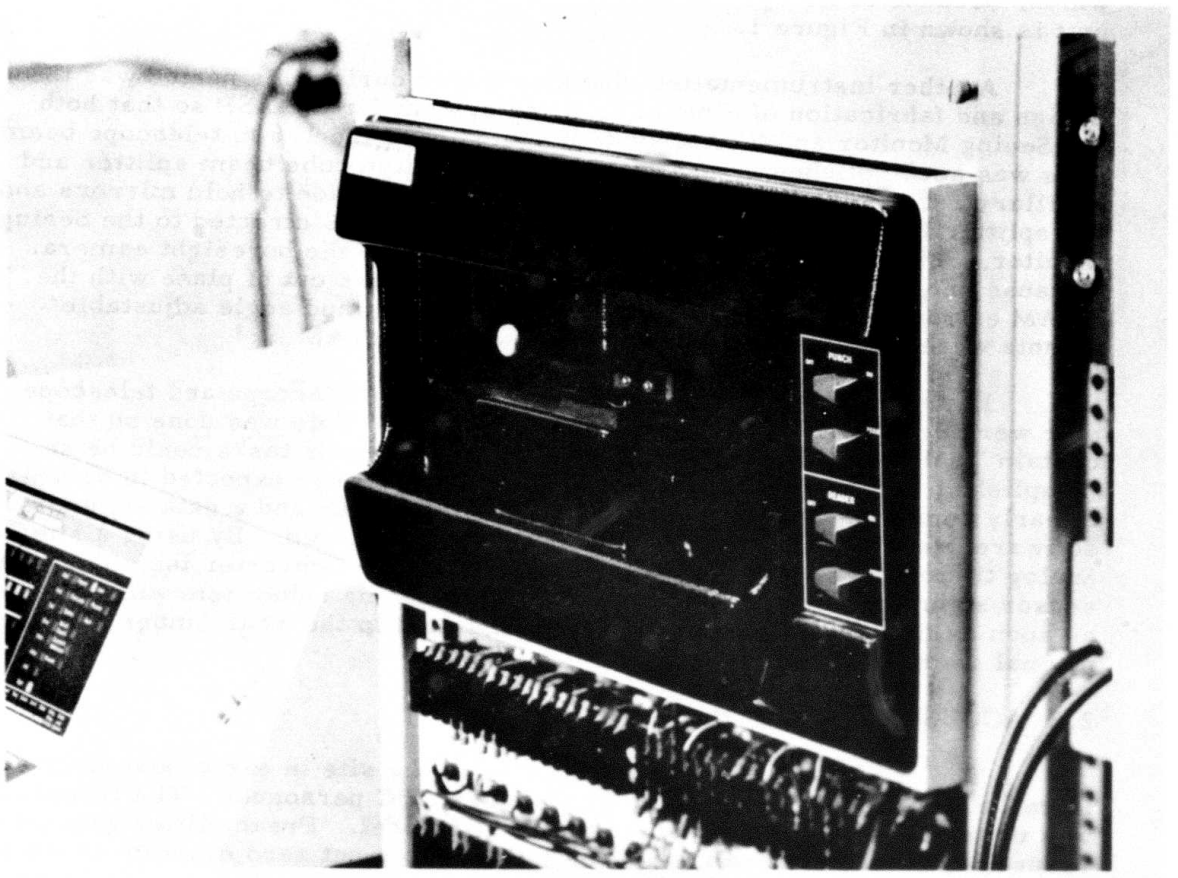

G9430

Figure 1 **The PC-04** Reader/Puncher Installed in the PDP-8I Computer

The new software package (Mk 5.0) has many added features. The most important is the "automated operation" which allows the sounder reduction program to continuously access the ambient temperature, dew point and barometric pressure as needed. This allows the reduction algorithm to use the most recent temperature, humidity and pressure data in the computation of the turbulence profile. In addition to retaining the voltmeter mode, which is invaluable for diagnostic work, an option is available that will output C_T^2 instead of C_n^2 values if desired. This feature will allow a fast comparison with microthermal probe data. Unfortunately, only the automated or non-automated mode function is controlled from the PDP-8I switch register, all other operational modes require software changes.

Because of the equipment changes made, a calibration constant in the program has to be modified. The constant has three multiplicative factors, two of which have already been determined. The first term is a power scaling effect resulting from upgrading the transducer from 40 W to 100 W. The second (also due to transducer changes) results from a loss in transducer efficiency. The last is a calibration factor between the microthermal probe and the sounder derived value of C_T^2. This term was measured by AFCRL.[4] Their calibration work, however, was at Jackass Flats, Nevada and not at AMOS. Simultaneous microthermal and acoustic sounder data is required to establish this factor.

The acoustic sounder work was halted in January of this year due to a failure in the automatic dewpoint system. The device is expected to be repaired early in the next quarter and calibration measurements between the sounder and microthermal probe systems can then be completed.

In order to take advantage of the features of the new Mk 5.0 software, a modest upgrade of the Bell & Howell VR3700B tape recorder will have to be made. With the present reproduce configuration of the recorder there is only one speed (15 ips) which will allow a four channel reproduce function. This arrangement has the drawback that at 15 ips it is not economical of tape and provides excessive bandwidth with the attendant increase in noise which in turn limits the maximum profile altitude attainable. The solution is to add four intermediate band reproduce amplifiers with compatible filters such that the acoustic sounder return, ambient temperature, dewpoint and barometric pressure can be recorded and played back simultaneously. Until these upgrades are accomplished, sounder data runs will be made using the non-automated procedures.

---

(4) D. P. Greenwood, D. O. Tarazano, D. A. Haugen, J. C. Kaimal, J. Newman, P. F. Kellen and M. G. Miller, AMOS Seeing Quality Measurements, Rome Air Development Center Technical Report #RADC-TR-75-295 (January 1976).

2.4 REAL TIME ATMOSPHERIC MEASUREMENT (RTAM) SYSTEM

2.4.1 Experimental Operations

The RTAM was returned to AMOS after some reconstruction and retesting at the factory. Principal changes made were to the optical train. The August 1976 tests[3] showed a significant degradation in performance due to chromatic aberration. This was overcome by replacing the original system's lens elements with well corrected (chromatic aberration) ones mounted in precise, adjustable mechanical mounts. The instrumental field of view was also significantly improved. The two channel, two photomultiplier system was converted to a two channel, one photomultiplier system. This resulted in a 50% reduction in duty cycle (from 4 ms to 8 ms for each successive value of X and Y). Finally, the phase processing electronics were modified.

Initial testing of the modified system occurred during late January. Bench tests with a He: Ne laser confirmed the electronic and optical integrity of the sensor. After a precise alignment of RTAM in the ASP, the package was mounted on the 1.6 m telescope as shown in Figure 2. Telescope tests indicated a lower than desired signal to noise ratio; hence, the RTAM sensor head was demounted and optimized for single channel operation. This was effected by readjusting the system elements to center the zero and first orders of the Y-channel in the sensor's optical train. This action, while increasing the signal to noise ratio in one channel, decreased it in the other. The system was remounted on the 1.6 m telescope and more observations against bright stars were carried out. Sufficient improvement was achieved by this optimization that system performance was deemed acceptable enough to attempt a verification of the Seeing Monitor's output via simultaneous data collection using the beam splitter system described in Section 2.2.

The dual instrument configuration mounted on the 1.6 m telescope is shown in Figure 3. Even with the favorable beam split (~70% to RTAM) it was necessary to use the brightest stars in the sky to achieve sufficient signal to noise ratio. These stars were Sirius, Procyon and Capella, giving a range in visual magnitude from -1.4 to 0.5. During the several nights of data collection, the RTAM outputs were recorded on magnetic tape with the VR-3700B recorder at maximum bandwidth. The Seeing Monitor analog seeing angle data were processed with compatible averaging times using the PDP-8I Means and Variance Program in real time.

2.4.2 Processing Electronics

The outputs of the RTAM are in the form of analog voltages which scan, in time, the modulus (MTF) and phase (PTF) of the combined atmosphere-telescope optical transfer function. As such, this data can, in principle, be used to provide a detailed characterization of these quantities. However, these outputs do not lend themselves to a real-time single parameter characterization of atmospheric seeing without further processing. To provide this type of information, analog processing electronics have been designed and

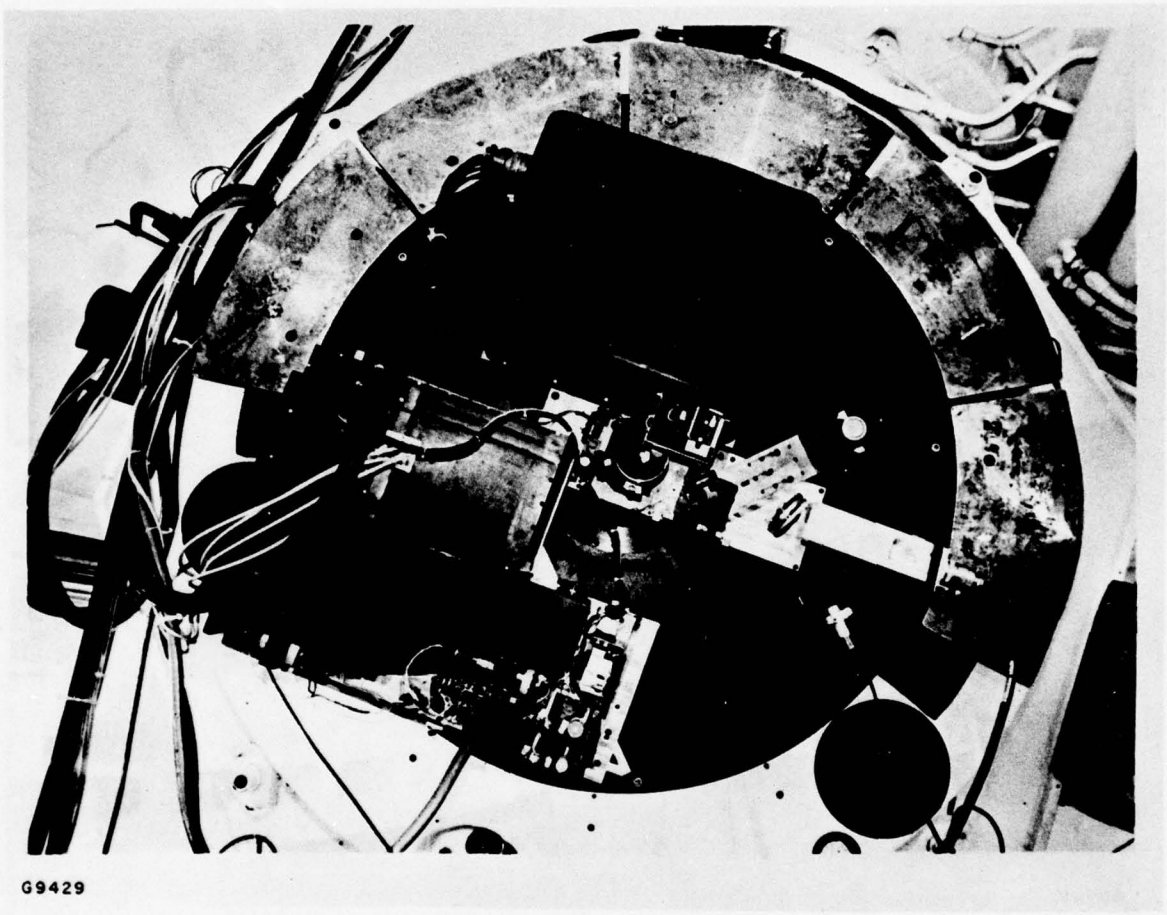

G9429

Figure 2 The ASP Containing Both the RTAM and Seeing Monitor, Mounted on the Rear Blanchard of the 1.6 m Telescope. The uppermost package is the RTAM. The lower one is the Seeing Monitor. The filter wheel and auxiliary optics are located in center of the photograph.

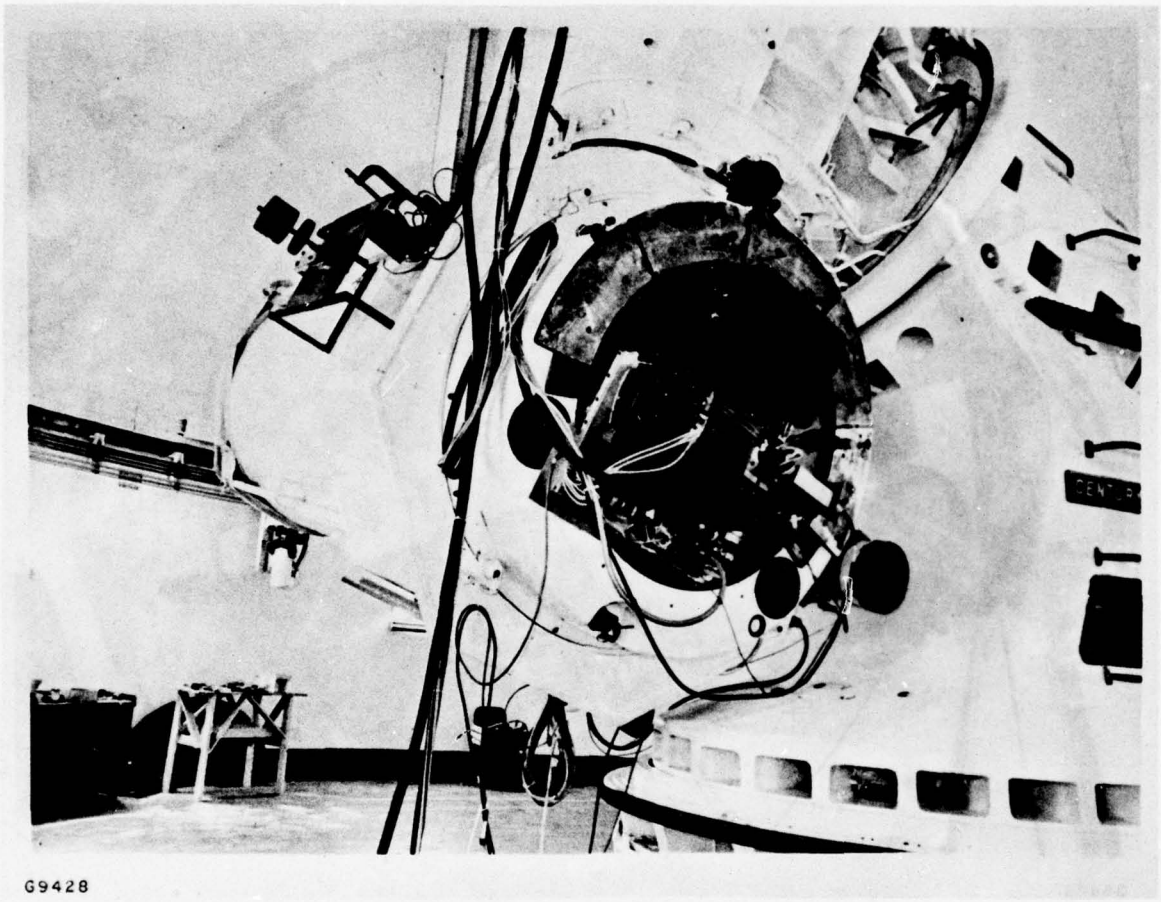

G9428

Figure 3 The RTAM/SM Package Mounted on the 1.6 m Telescope

fabricated. The concept implemented is to determine the time (spatial frequency) at which the MTF drops to a prescribed fraction of its initial (zero frequency) value, nominally 0.5. A PDP-8 compatible analog voltage proportional to this time is developed and held until the next MTF appears. This processing technique is essentially equivalent to internal electronics in the SM and, hence, the averaged outputs of the two devices should yield very comparable data.

The basic principle of operation of the electronics centers around a sample and hold technique. The observed signal is alternately sampled and held through a unity gain amplifier using a constant sampling frequency. The sample and hold amplifier's output is continuously compared with its input during the hold interval. As shown in Figure 4, during the entire time when the amplifier's input amplitude is greater than or equal to its output, the waveform is either rising or at the top of its peak. At the instant when the amplifier's input drops below its output, the signal peak has been reached and is beginning its descent.

Because the process of peak detection is non-anticipatory, it is impossible to actually detect a peak until it has passed. Therefore, the accuracy of the represented peak value given must be resolved to the greatest extent possible using the degrees of freedom available. The factors affecting the system's accuracy are signal bandwidth and fall time characteristics, signal waveshape, sampling frequency, sample and hold amplifier speed and accuracy, and differential comparator speed and accuracy. The problem of obtaining peak signal accuracy is nearly eliminated in the case of a system having waveforms of constant fall time. Here, it would only be necessary to add a fixed bias offset to the detected output signal. In all other cases where the detector must function under varying signal conditions, one must select a suitable sampling frequency and appropriate components to restrict the overall system error to within certain bounds over the detection bandwidth.

Figure 5 shows a block diagram of the peak detector circuit with its basic components. The threshold sense comparator whose preset reference level determines the operating interval is used to inhibit operation and reset all applicable circuit functions at points below the sensing threshold. This may be desirable if there are unwanted low level perturbations on the baseline which might otherwise cause false detection as shown in Figure 6.

A block diagram of one channel of the complete processing electronics package is shown in Figure 7, while Figure 8 shows the timing diagram. A detailed schematic of the peak detection circuit is given in Figure 9. Two input buffers are required due to the current requirements of the sample and hold. The 1 MHz sampling clock is used to provide a one microsecond detection time resolution.

The completed package is shown in Figure 10. It includes two channels which are identical except for a fixed timing offset corresponding to the alternating RTAM channel x and y MTF outputs. A functional description is given below.

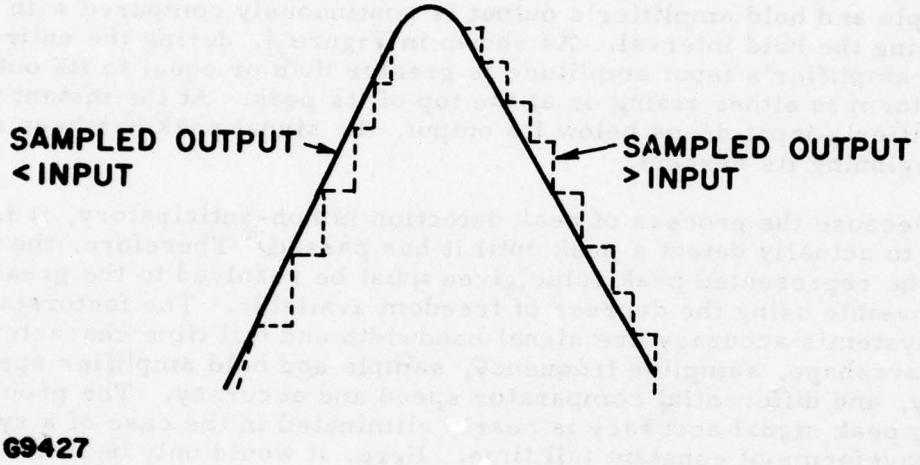

Figure 4 Peak Detection Principle

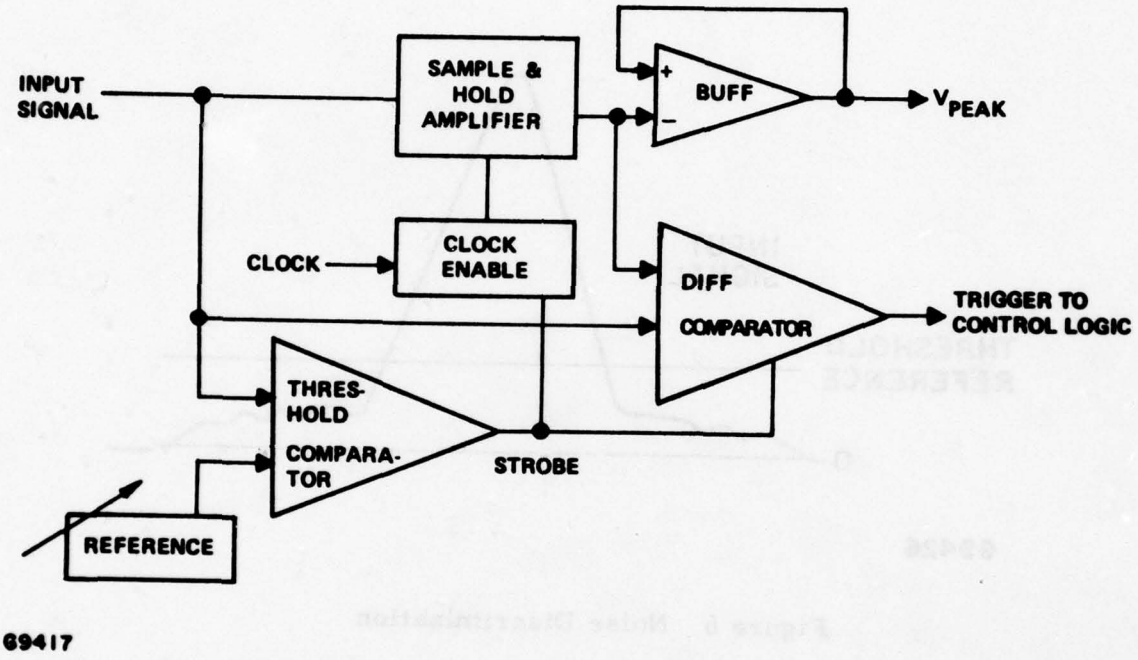

Figure 5 Peak Detector Block Diagram

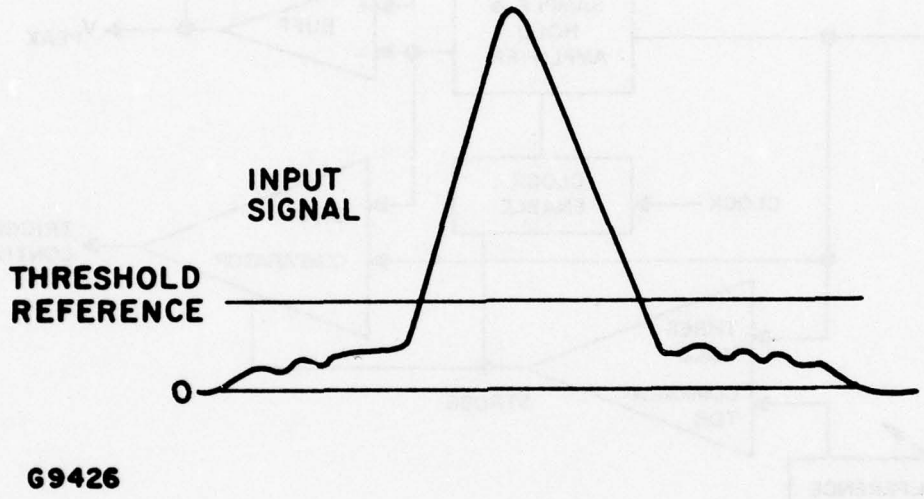

Figure 6 Noise Discrimination

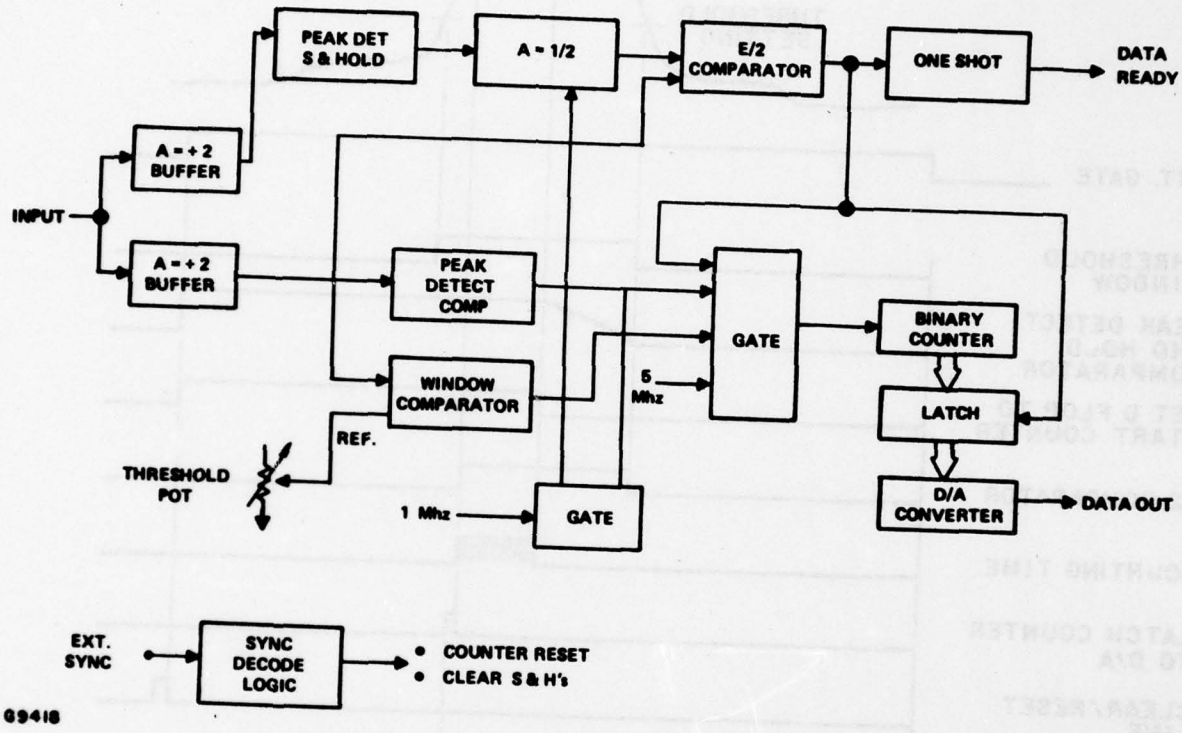

Figure 7 Processing Electronics Block Diagram

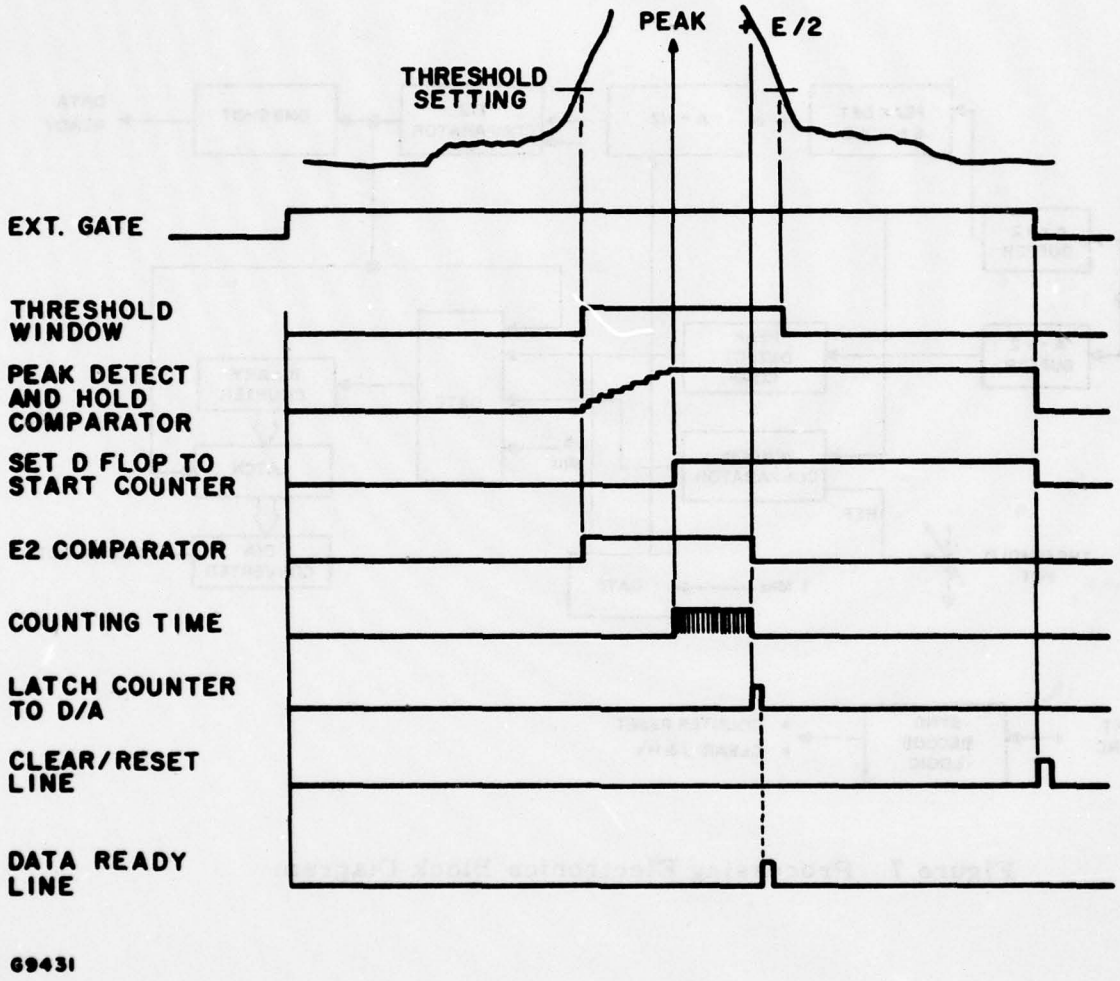

Figure 8 Processing Electronics Timing Diagram

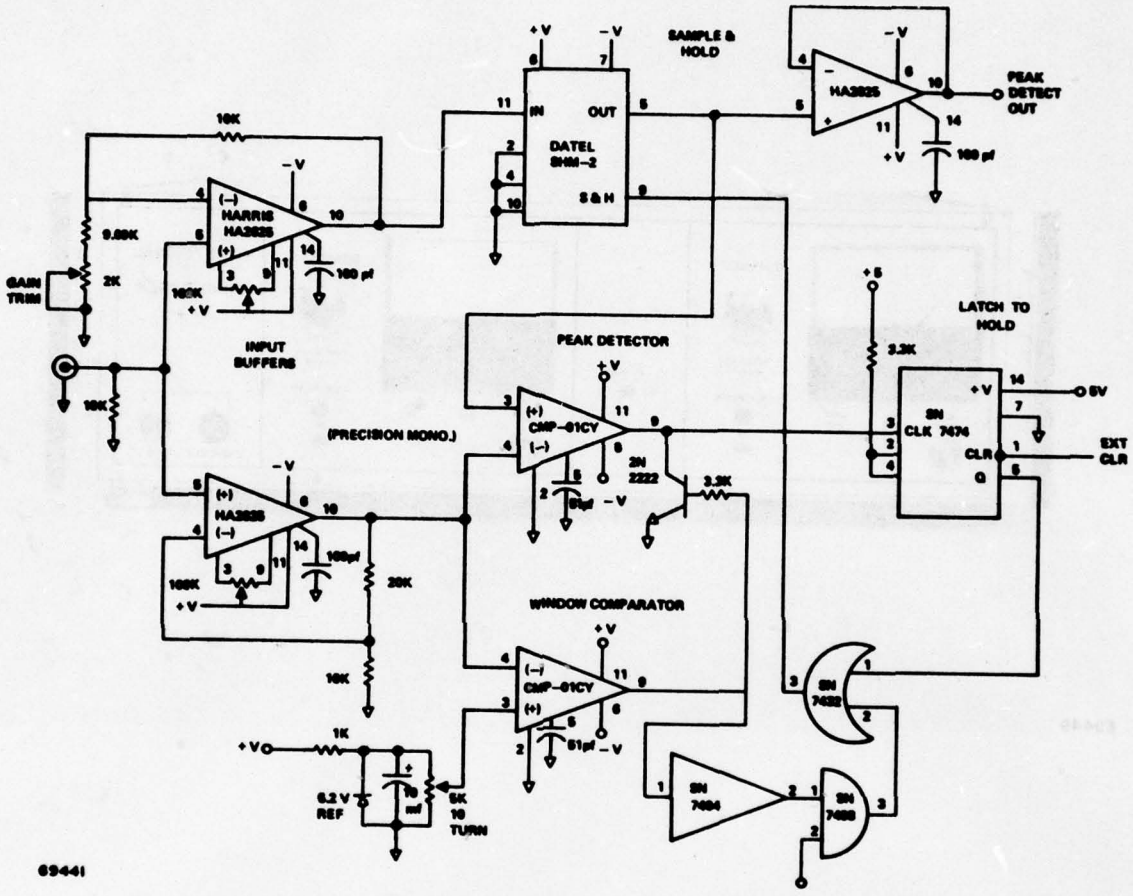

Figure 9 Peak Detector Schematic

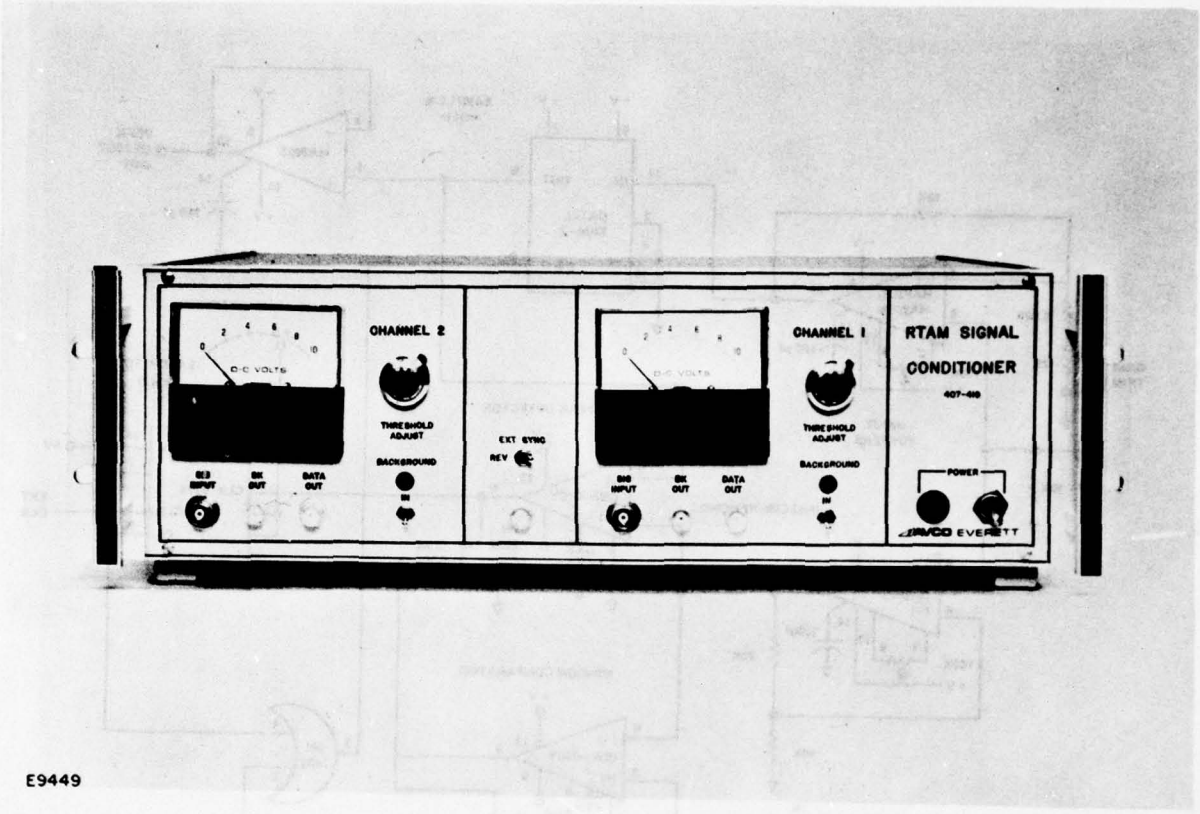

E9449

Figure 10 RTAM Processing Electronics

AC Power 'ON' Switch:

Powers complete chasis when the switch is 'ON'.

Panel Meter:

(0-10 VFS) calibrated to 0-200 μsec. Buffered from the data output signals.

Data Output (front panel BNC):

The data output signal is a DC voltage whose value is equivalent to the time between the peak and peak/2 value of the input signal. A calibration curve is given in Figure 11. The conversion factor is .489 volts/10 μsec. Data output range is 0 to +10 volts. Data output sourcing capability is +5 mA maximum (short circuit proof). Load impedance should be 100 k ohms or greater to maintain measurement accuracy.

Sync (rear panel BNC):

The sync is a TTL negative true logic output signal (10 μsec wide) available for external use. Data output is stable at the trailing edge of the sync signal. The TTL sync signal has the capability to drive 50 ohm cable.

1 MHz Output (rear panel BNC):

A TTL reference signal for external timing (if required). This signal is derived from the internal 5 MHz master oscillator. The 1 MHz output has 50 ohm drive capability.

Bk (background) Output Signal (front panel BNC):

The background signal is a DC voltage (scaled up by x 10) representative of a sample taken of the input line prior to the arrival of the main signal. The range is 0 ± 10 volts R_L = 2k or greater and is always available; however, the external sync must be provided for proper operation.

Background Switch (front panel toggle switch):

With the background switch in the 'IN' position internal circuitry is enabled so that background is cancelled in the determination of the peak and E/2 values of the input signal. When the switch is in the disabled position (i.e., LED indicator lamp out) no background cancellation is provided although the background is still sampled and available as an output signal.

External Sync Input (front panel BNC):

TTL compatible logic buffered input. Normally the RTAM x-gate output is connected to this input. The external sync logic signal is required to properly align the Channel 1 and Channel 2 data and background signals.

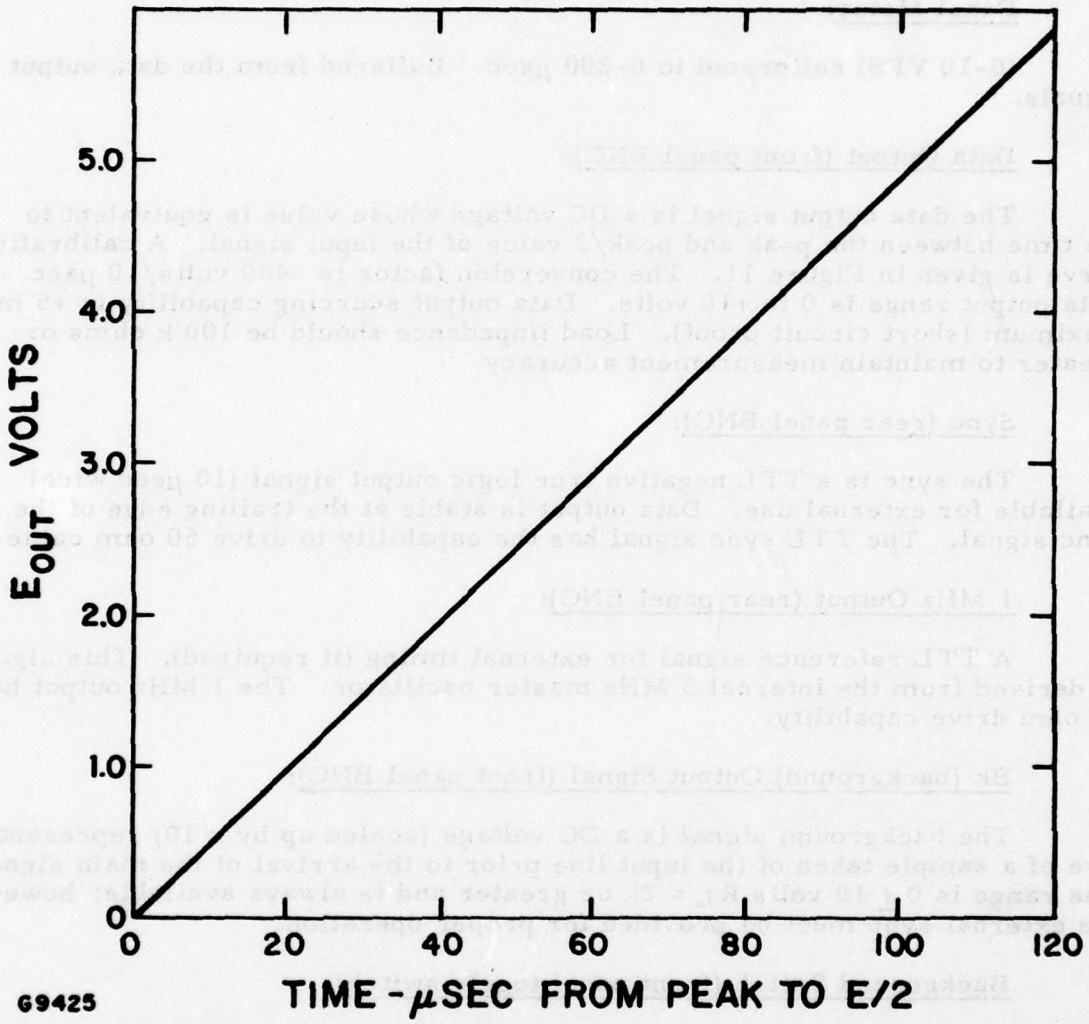

Figure 11 Processing Electronics Calibration Curve

External Sync - Reversal Switch - (front panel toggle switch):

The switch gives the ability to reverse (or not) the phase of the external sync signal after it is decoded. With the switch in the correct position, proper alignment will be maintained between sync and input data signals.

Data Input (front panel BNC):

High impedance input for RTAM channel x (channel 1) and channel y (channel 2) MTF signals.

Threshold Adjustment (front panel potentiometer):

The threshold adjustment establishes a window, in which internal circuitry is enabled to determine the peak of the input, E/2 value, gating and reset times. The potentiometer calibration scale is 0.5 volts/turn. The threshold value should be set at a value which is greater than the background noise level prior to the signal.

3.0 EXPERIMENTAL DATA AND ANALYSIS

3.1 ACOUSTIC SOUNDER AND MICROTHERMAL DATA

Prior to the failure of the automatic dewpoint system some test runs of the acoustic sounder were made in late December and early January. Although uncalibrated against the microthermal probes the results were the first data reduced using the new hardware and software configurations. Results obtained on 10 December 1976 are shown in Figure 12. The mission was run in the evening between the hours of 2000 and 2300, the sky was partly cloudy and there were light winds. The data shown probably represent the C_n^2 profile to 300 m within a factor or two or three; however, system noise which is shown as an equivalent C_n^2 profile, dominates the higher altitudes. The two profiles shown are separated by approximately one hour in time. The lower portions of the curves are fairly linear but do not exhibit the (-2/3) or (-4/3) slope predicted by theory.(5) Data previously collected at AMOS(4) indicated, on the average, a (-1.4) slope. For comparative purposes, straight lines with these three slopes are indicated in the figure.

In January the six tower mounted probes were rebuilt and several data runs were made under day and night conditions. These initial operations produced long term values of probe variances which were used for smoothing the PDP-8I scaling factors. Although it was not possible to complete the calibration of the acoustic sounder the reasons stated above, some probe data were reduced for general systems evaluation. The probes outputs are sampled by the PDP-8I computer which calculates the required variances and covariances. These data are then used to obtain the desired estimated of C_T^2 and C_n^2. The sampling periods are typically ten minutes in length.

Figure 13 shows C_T^2 histories for the north and south towers during the afternoon of 13 March 1977. Three comparison points representing nightly averages for both towers during the November 1975 test period are shown as the lower curve. The daytime data indicate higher temperature turbulence as might be expected.

3.2 SEEING MONITOR DATA AND ANALYSIS

3.2.1 Routine Data

During the period 15 September 1976 to 15 March 1977 data was successfully collected on ten occasions. The results are summarized in

(5) J.C. Wyngaard, J. Izumi and S.A. Collins, Jr., Behavior of the Refractive-Index-Structure Parameter Near the Ground, J. Opt. Soc. Am. 61, 1646 (1971).

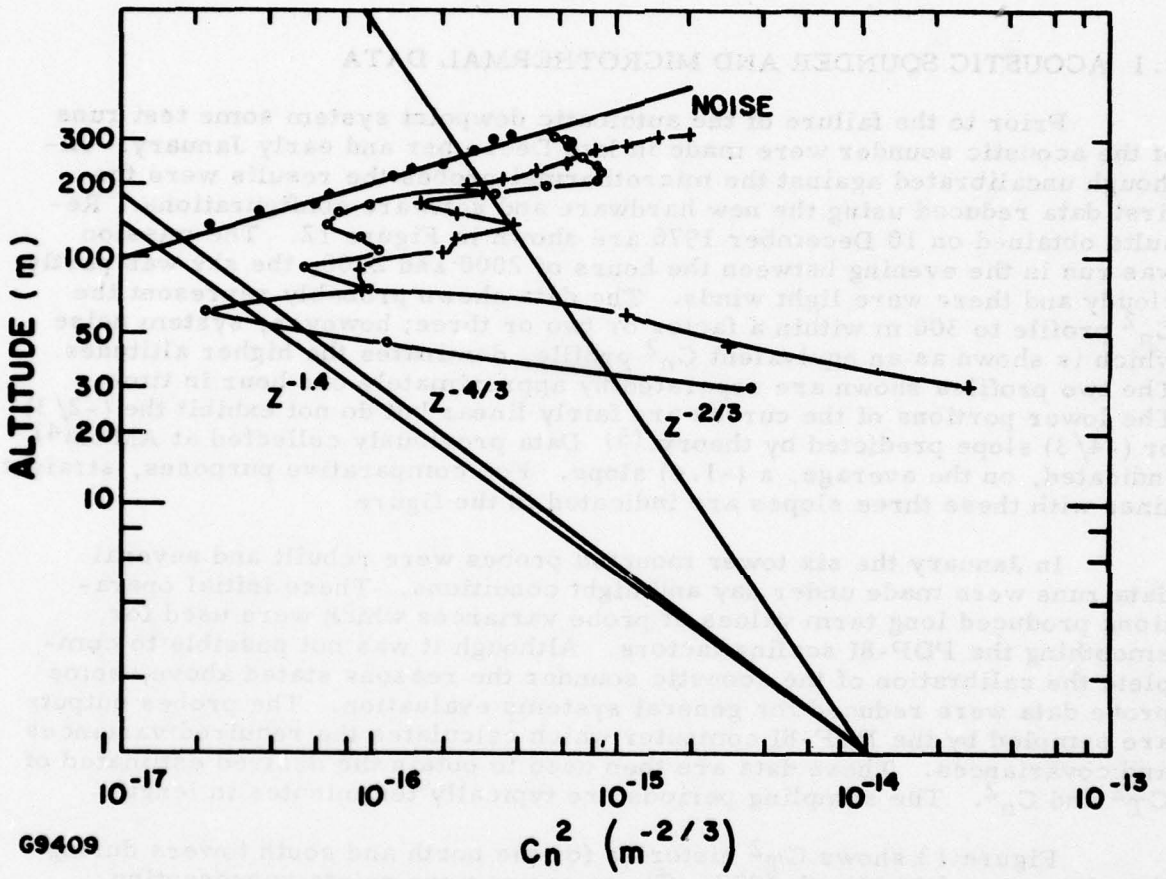

Figure 12 Acoustic Sounder C_n^2 Profile of 10 December 1976

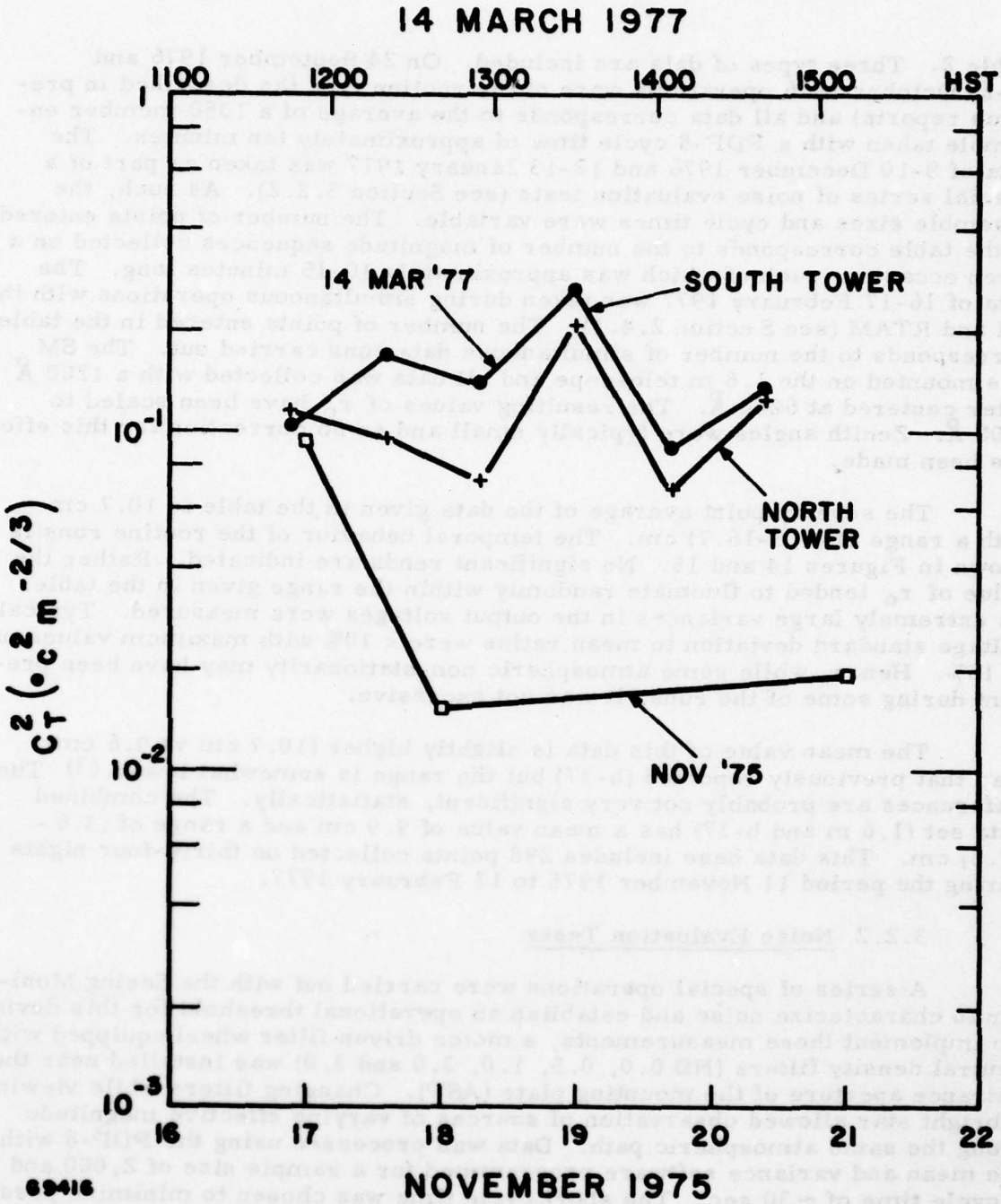

Figure 13 Microthermal Probe C_T^2 Histories for the Afternoon of 14 March 1977 (Top Scale) and Evenings of 17, 18 and 21 November 1975 (Bottom Scale)

Table 2. Three types of data are included. On 24 September 1976 and 27-29 October 1976 operations were of the routine type (as described in previous reports) and all data corresponds to the average of a 1350 member ensemble taken with a PDP-8 cycle time of approximately ten minutes. The data of 9-10 December 1976 and 12-13 January 1977 was taken as part of a special series of noise evaluation tests (see Section 3.2.2). As such, the ensemble sizes and cycle times were variable. The number of points entered in the table corresponds to the number of magnitude sequences collected on a given occasion, each of which was approximately 10-15 minutes long. The data of 16-17 February 1977 was taken during simultaneous operations with the SM and RTAM (see Section 2.4.1). The number of points entered in the table corresponds to the number of simultaneous data runs carried out. The SM was mounted on the 1.6 m telescope and all data was collected with a 1200 Å filter centered at 6200 Å. The resulting values of r_o have been scaled to 5000 Å. Zenith angles were typically small and so no correction for this effect has been made.

The seventy point average of the data given in the table is 10.7 cm with a range of (3.6-16.7) cm. The temporal behavior of the routine runs is shown in Figures 14 and 15. No significant rends are indicated. Rather the value of r_o tended to fluctuate randomly within the range given in the table. No extremely large variances in the output voltages were measured. Typical voltage standard deviation to mean ratios were < 10% with maximum values of ~ 15%. Hence, while some atmospheric non-stationarity may have been present during some of the runs, it was not excessive.

The mean value of this data is slightly higher (10.7 cm vs 9.6 cm) than that previously reported (b-37) but the range is somewhat lower.[3] The differences are probably not very significant, statistically. The combined data set (1.6 m and b-37) has a mean value of 9.9 cm and a range of (3.6 - 17.8) cm. This data base includes 298 points collected on thirty-four nights during the period 11 November 1975 to 17 February 1977.

3.2.2 Noise Evaluation Tests

A series of special operations were carried out with the Seeing Monitor to characterize noise and establish an operational threshold for this device. To implement these measurements, a motor driven filter wheel equipped with neutral density filters (ND 0.0, 0.5, 1.0, 2.0 and 3.0) was installed near the entrance aperture of the mounting plate (ASP). Changing filters while viewing a bright star allowed observation of sources of varying effective magnitude along the same atmospheric path. Data was processed using the PDP-8 with the mean and variance software programmed for a sample size of 2,000 and a cycle time of ~ 30 sec. The short cycle time was chosen to minimize possible temporal non-stationarity effects. An experimental assessment of these effects was obtained by cycling the filters in a contiguous fashion during a given data run. An example of one such cycle used was 0.0; 0.5; 0.0; 0.5; 1.0; 0.5; 1.0; 2.0; 1.0; 2.0; 3.0; 2.0; 3.0. This run took ~ 12.5 minutes to complete. The Seeing Monitor was mounted on the 1.6 m telescope and operated in the usual fashion with a 1200 Å bandpass at 6200 Å central wavelength.

TABLE 2. SEEING MONITOR DATA SUMMARY

Date	Time Period HST	No. of Points	r_o at 5000Å; cm Mean	Range
24 Sept 1976	0240 - 0510	15	5.0	3.6 - 6.2
27 Oct 1976	2000 - 2320	7	12.8	11.9 - 13.5
28 Oct 1976	1950 - 2320	14	13.2	10.9 - 14.9
29 Oct 1976	1840 - 2310	12	11.8	8.2 - 13.6
9 Dec 1976	1330	1	14.6	---
10 Dec 1976	1900 - 2100	7	14.0	12.0 - 16.7
12 Jan 1977	1940 - 2220	6	11.4	10.3 - 17.6
13 Jan 1977	2150 - 2250	5	12.3	11.0 - 15.3
16 Feb 1977	---	1	5.4	---
17 Feb 1977	---	2	5.6	---

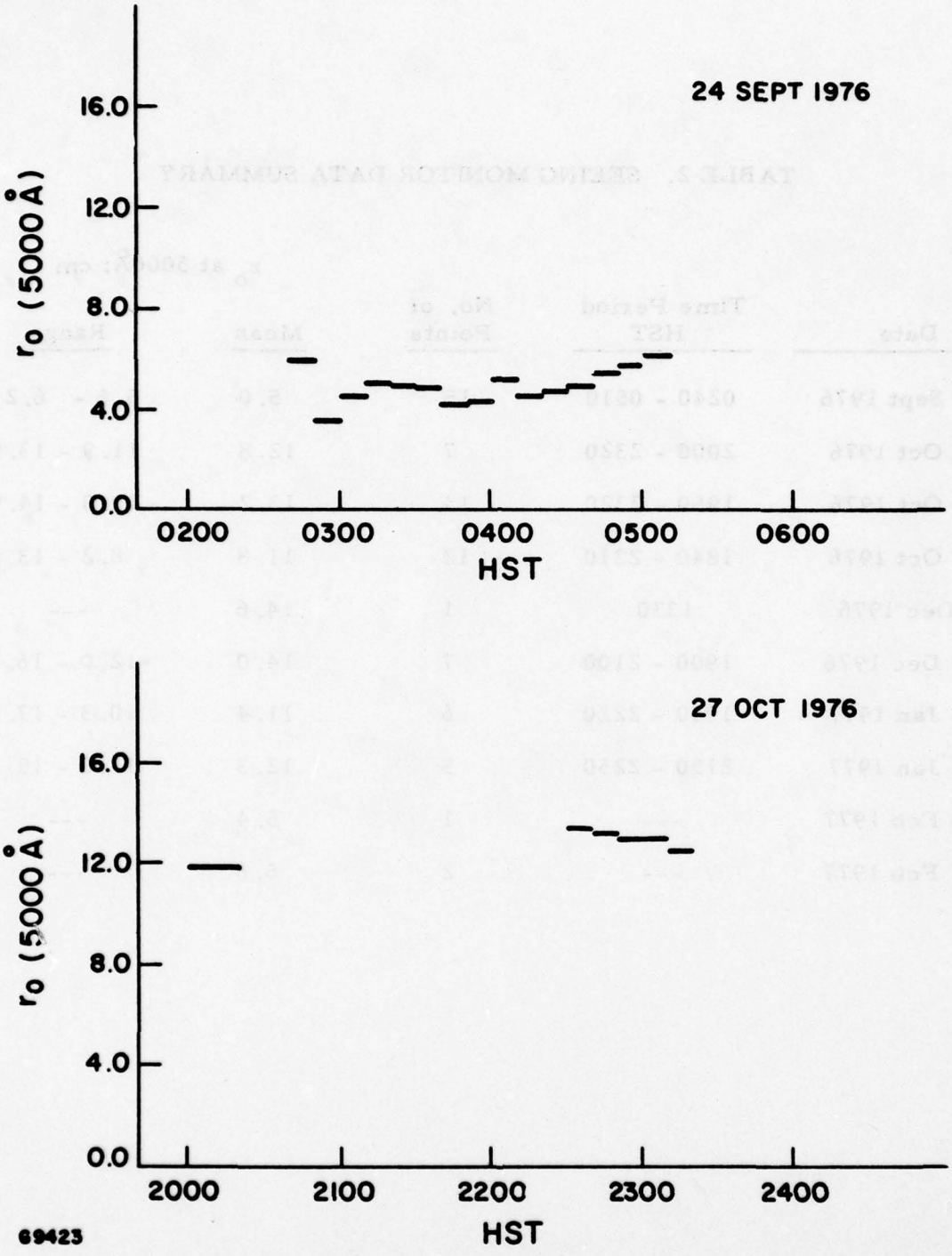

Figure 14 Seeing Monitor Data of 24 September and 27 October 1976. The horizontal bars indicate the averaging period.

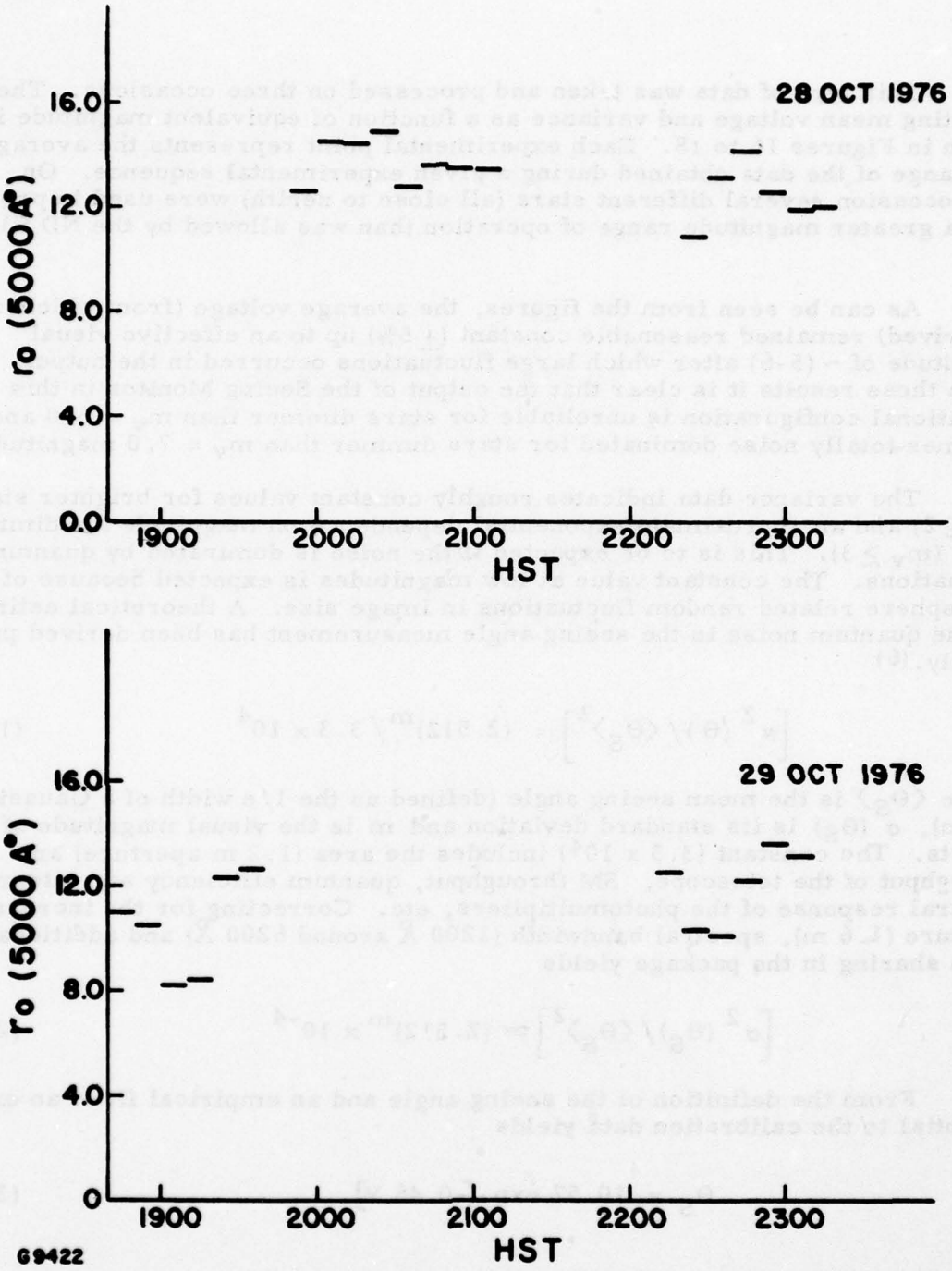

Figure 15 Seeing Monitor Data of 28 and 29 October 1976. The horizontal bars indicate the averaging period.

This type of data was taken and processed on three occasions. The resulting mean voltage and variance as a function of equivalent magnitude is shown in Figures 16 to 18. Each experimental point represents the average and range of the data obtained during a given experimental sequence. On each occasion several different stars (all close to zenith) were used to provide a greater magnitude range of operation than was allowed by the ND filters.

As can be seen from the figures, the average voltage (from which r_o is derived) remained reasonable constant ($\pm$ 5%) up to an effective visual magnitude of ~ (5-6) after which large fluctuations occurred in the output. From these results it is clear that the output of the Seeing Monitor in this operational configuration is unreliable for stars dimmer than $m_v = 5.0$ and becomes totally noise dominated for stars dimmer than $m_v = 7.0$ magnitude.

The variance data indicates roughly constant values for brighter stars ($m_v \lesssim 2$) and an approximate exponential dependence on magnitude for dimmer stars ($m_v \gtrsim 3$). This is to be expected if the noise is dominated by quantum fluctuations. The constant value at low magnitudes is expected because of the atmosphere related random fluctuations in image size. A theoretical estimate for the quantum noise in the seeing angle measurement has been derived previously.(6)

$$\left[\sigma^2(\theta)/\langle\theta_S\rangle^2\right] = (2.512)^m/3.3 \times 10^4 \qquad (1)$$

where $\langle\theta_S\rangle$ is the mean seeing angle (defined as the 1/e width of a Gaussian image), $\sigma(\theta_S)$ is its standard deviation and m is the visual magnitude of the objects. The constant (3.3×10^4) includes the area (1.2 m aperture) and throughput of the telescope, SM throughput, quantum efficiency and integrated spectral response of the photomultipliers, etc. Correcting for the increase in aperture (1.6 m), spectral bandwidth (1200 Å around 6200 Å) and additional beam sharing in the package yields

$$\left[\sigma^2(\theta_S)/\langle\theta_S\rangle^2\right] \simeq (2.512)^m \times 10^{-4} \qquad (2)$$

From the definition of the seeing angle and an empirical fit of an exponential to the calibration data yields

$$\theta_S = 10.57 \exp\left[-0.46\ V\right] \qquad (3)$$

(6) G.R. Giuliano, J.A. Jenney, L. Miller, M.E. Pedinoff, D.Y. Tseng and S.M. Wandzura, Space Object Imaging, Final Technical Report, Contract F30602-74-C-0227 (Hughes Research Laboratories), Rome Air Development Center Technical Report #RADC-TR-76-54 (March 1976).

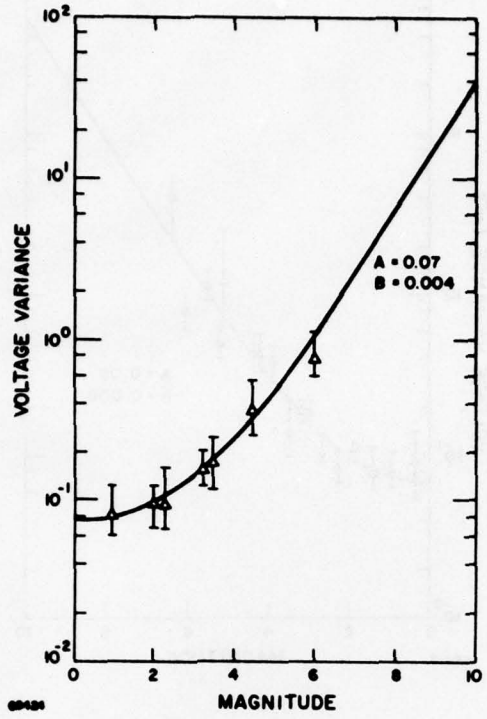

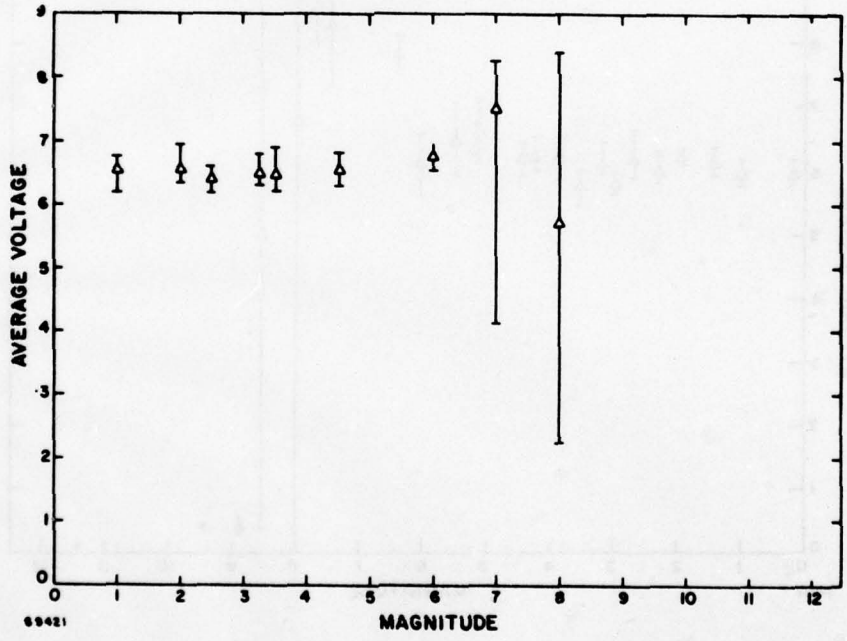

Figure 16 Seeing Monitor Noise Characterization Data of 10 December 1976

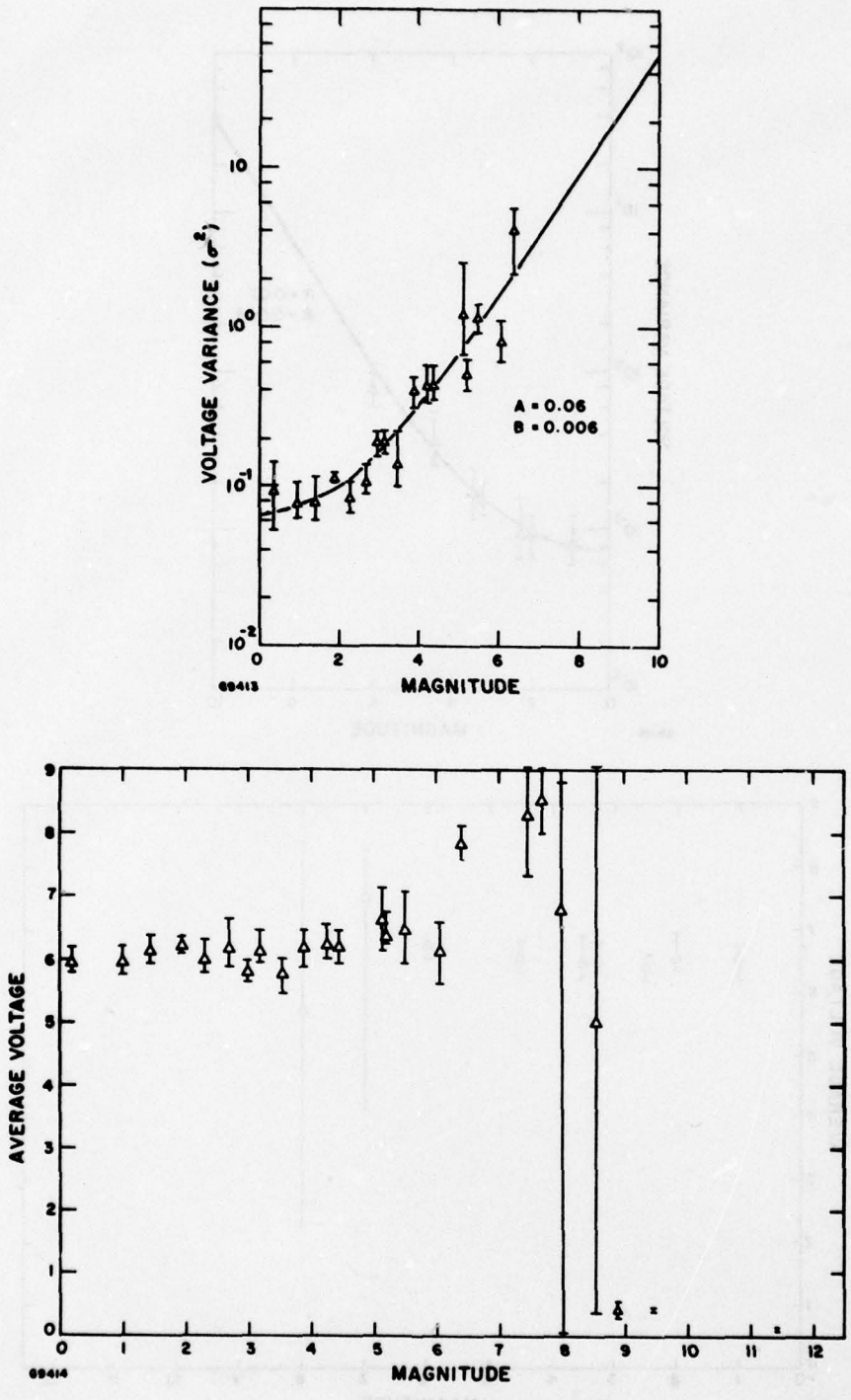

Figure 17 Seeing Monitor Noise Characterization Data of 12 January 1977

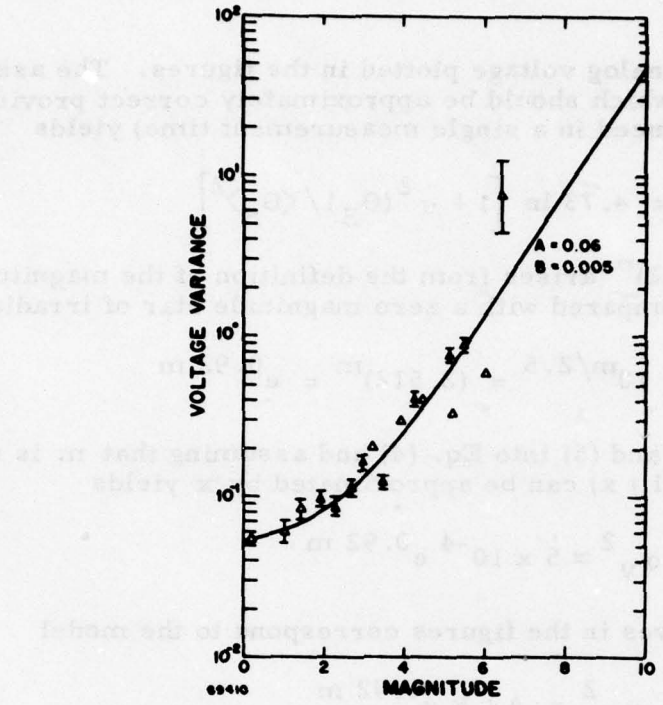

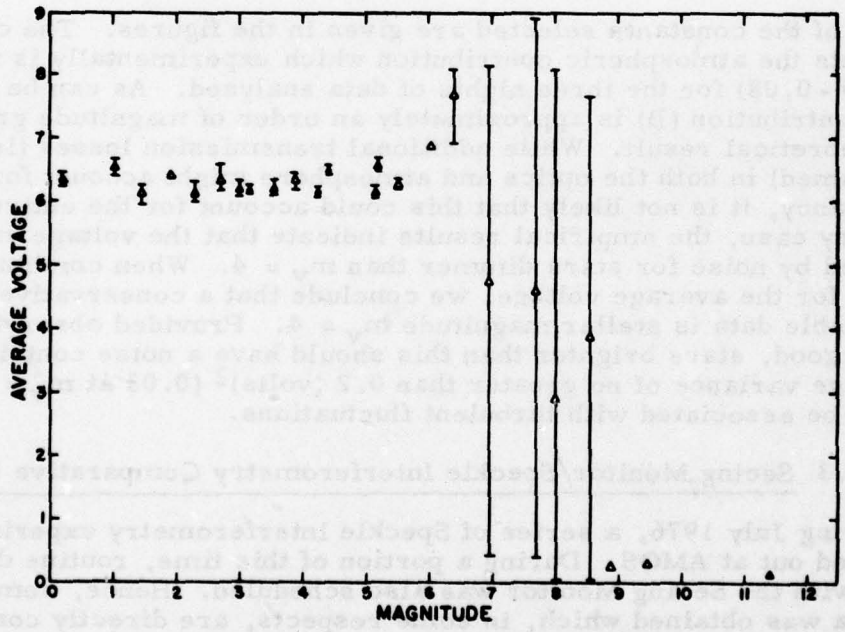

Figure 18 Seeing Monitor Noise Characterization Data of 13 January 1977

where V is the output analog voltage plotted in the figures. The assumption of Gaussian statistics (which should be approximately correct provided many photoelectrons are produced in a single measurement time) yields

$$\sigma_V^2 = 4.73 \ln \left[1 + \sigma^2(\Theta_S)/\langle\Theta_S\rangle^2\right] \quad (4)$$

The factor $(2.512)^m$ arises from the definition of the magnitude of a star of irradiance H compared with a zero magnitude star of irradiance H_o.

$$(H/H_o) = 10^{m/2.5} = (2.512)^m = e^{0.92\,m} \quad (5)$$

Substitution of Eqs. (2) and (5) into Eq. (4) and assuming that m is small enough ($\lesssim 8$) so that ln (1 + x) can be approximated by x yields

$$\sigma_V^2 \simeq 5 \times 10^{-4}\, e^{0.92\,m} \quad (6)$$

The smooth curves in the figures correspond to the model

$$\sigma_T^2 = A + B\, e^{0.92\,m} \quad (7)$$

The values of the constants selected are given in the figures. The constant A represents the atmospheric contribution which experimentally is in the range (0.05 - 0.08) for the three nights of data analyzed. As can be seen, the noise contribution (B) is approximately an order of magnitude greater than the theoretical result. While additional transmission losses (in excess of that assumed) in both the optics and atmosphere might account for part of the discrepancy, it is not likely that this could account for the entire difference. In any case, the empirical results indicate that the voltage variance is dominated by noise for stars dimmer than $m_v = 4$. When combined with the results for the average voltage, we conclude that a conservative threshold for reliable data is stellar magnitude $m_v = 4$. Provided observing conditions are good, stars brighter than this should have a noise contribution to the voltage variance of no greater than 0.2 $(\text{volts})^2$ (0.03 at $m_v = 2$). The excess can be associated with turbulent fluctuations.

3.2.3 Seeing Monitor/Speckle Interferometry Comparative Data

During July 1976, a series of Speckle Interferometry experiments were carried out at AMOS. During a portion of this time, routine data collection with the Seeing Monitor was also scheduled. Hence, some overlapping data was obtained which, in some respects, are directly comparable. For these operations, the Speckle Interferometer was mounted on the 1.6 meter telescope and the SM was mounted on the b-37 (1.2 meter) telescope. Estimates of r_o from the SM were obtained in the usual fashion, i.e., 10 minute cycles with on-line PDP-8 data processing with all results scaled to 5000 Å.

Briefly, the technique of Speckle Interferometry[7] involves the collection of multiple frames of short exposure data which are processed in the spatial frequency plane. While SI was originally developed as an astronomical measurement technique, it is also well suited for obtaining atmospheric seeing data. The instrument used to make these measurements is described in detail elsewhere.[8] A schematic of its major components is shown in Figure 19 and include: (1) an optical train consisting of an enlarging lens, image rotators, a grating for wavelength selection and dispersion correction and a bandwidth selecting element; (2) a gated SIT video tube whose output consists of the integrated intensity along 500 scan lines and; (3) a dedicated NOVA computer system for data storage, processing and display.

For the case of interest here, data processing involves Fourier transforming a sequence of short exposure single or binary star images (typically two hundred) and averaging the squared modulus of the resulting data. For single stars, this just yields the second moment of the MTF (i.e., modulus of the optical transfer function). The resolution of the instrumental package is such that one hundred and fifty data points are obtained in the frequency plane. This allows a detailed comparison of theory and experiment. For both single and binary stars the relevant theory has been developed by Korff.[9] For low spatial frequencies (< atmospheric limit $\sim r_o$), the theory has as an asymptotic limit, the square of the Fried short exposure (wander removed) average MTF.[10] This is not surpirsing because the process of squaring the complex OTF automatically eliminates overall image wander. Hence, fitting the SI data to theory at low frequencies yields an estimate of r_o which is closely related to the estimate obtained with the Seeing Monitor. Binary data can also be used by simply dividing the results by the fringe pattern arising from the two point nature of the source, the period of which can be determined very accurately from the entire transform. This also yields an empirical estimate of the second moment of the MTF. An important point is that the determination of r_o from SI is based on a multi-point fit of the data to theory whereas the SM value is a single point fit (half MTF point). Hence, the SI data not only yields a single parameter (r_o) characterization of atmospheric seeing but also information on the consistency of the theoretical and empirical results.

Figure 20 shows an example of the fit of the data to low frequency theory. The experimental, normalized modulus-squared MTF ($\hat{\phi}$) divided by the square of the telescope MTF (τ_o) is plotted against ($q^{5/3} - q^2$) where q is the normalized spatial frequency ($\lambda f/D$ where f is spatial frequency, λ is wavelength and D is the telescope aperture size). q is equal to one at the

(7) J.C. Dainty, Stellar Speckle Interferometry, in Laser Speckle and Related Phenomena, Topics in Applied Physics Vol. 9, Ed. by J.C. Dainty (Springer-Verlag, Berlin, 1975).

(8) A.M. Schneiderman and D.P. Karo, How to Build a Speckle Interferometer, Proc. of SPIE, 75, 70 (1976).

(9) D. Korff, Analysis of a Method for Obtaining Near Diffraction Limited Information in the Presence of Atmosphere Turubulence, J. Opt. Soc. Am. 63, 971 (1973).

(10) D.L. Fried, Optical Resolution Through a Randomly Inhomogeneous Medium for Very Long and Very Short Exposures, J. Opt. Soc. Am. 56, 1372 (1966).

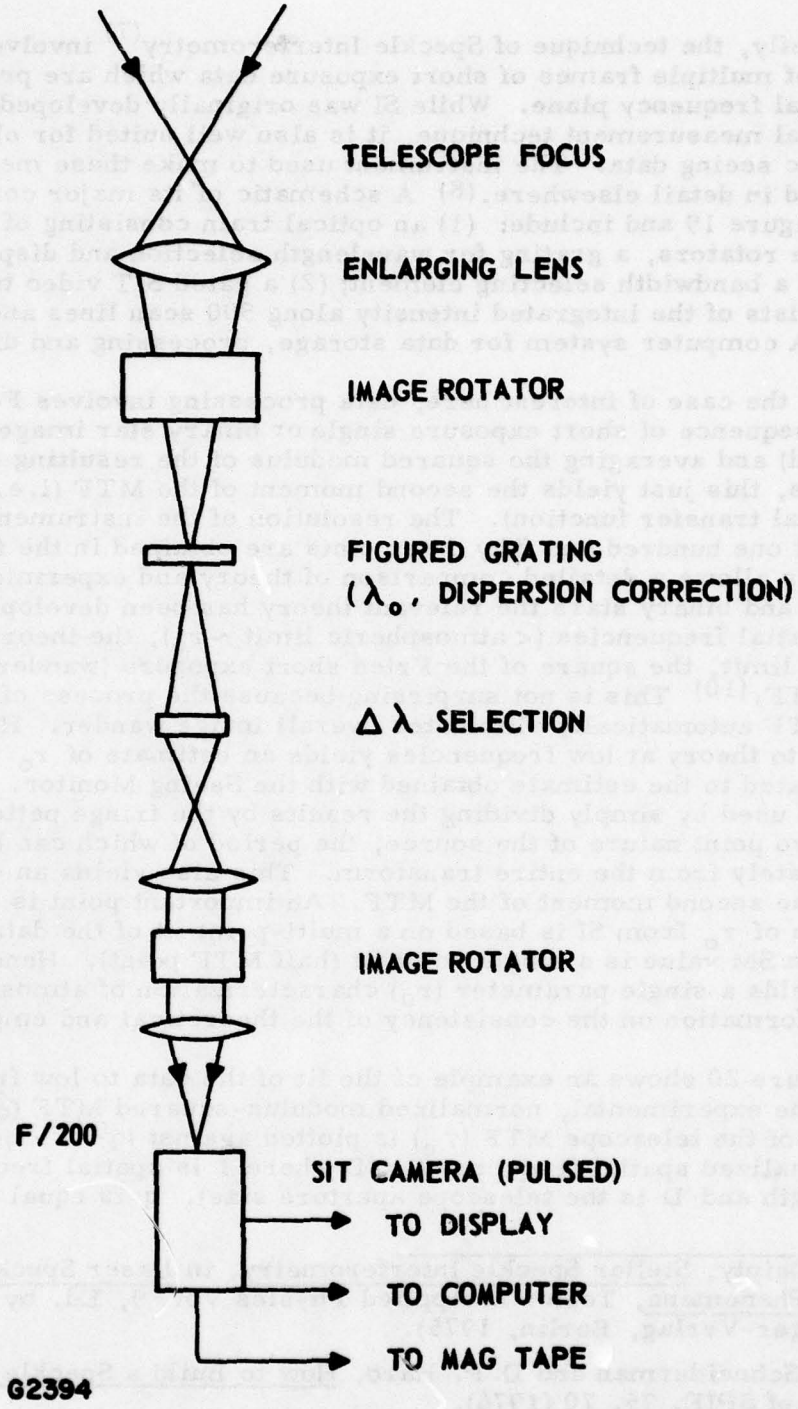

Figure 19 Speckle Interferometer - Optical Train

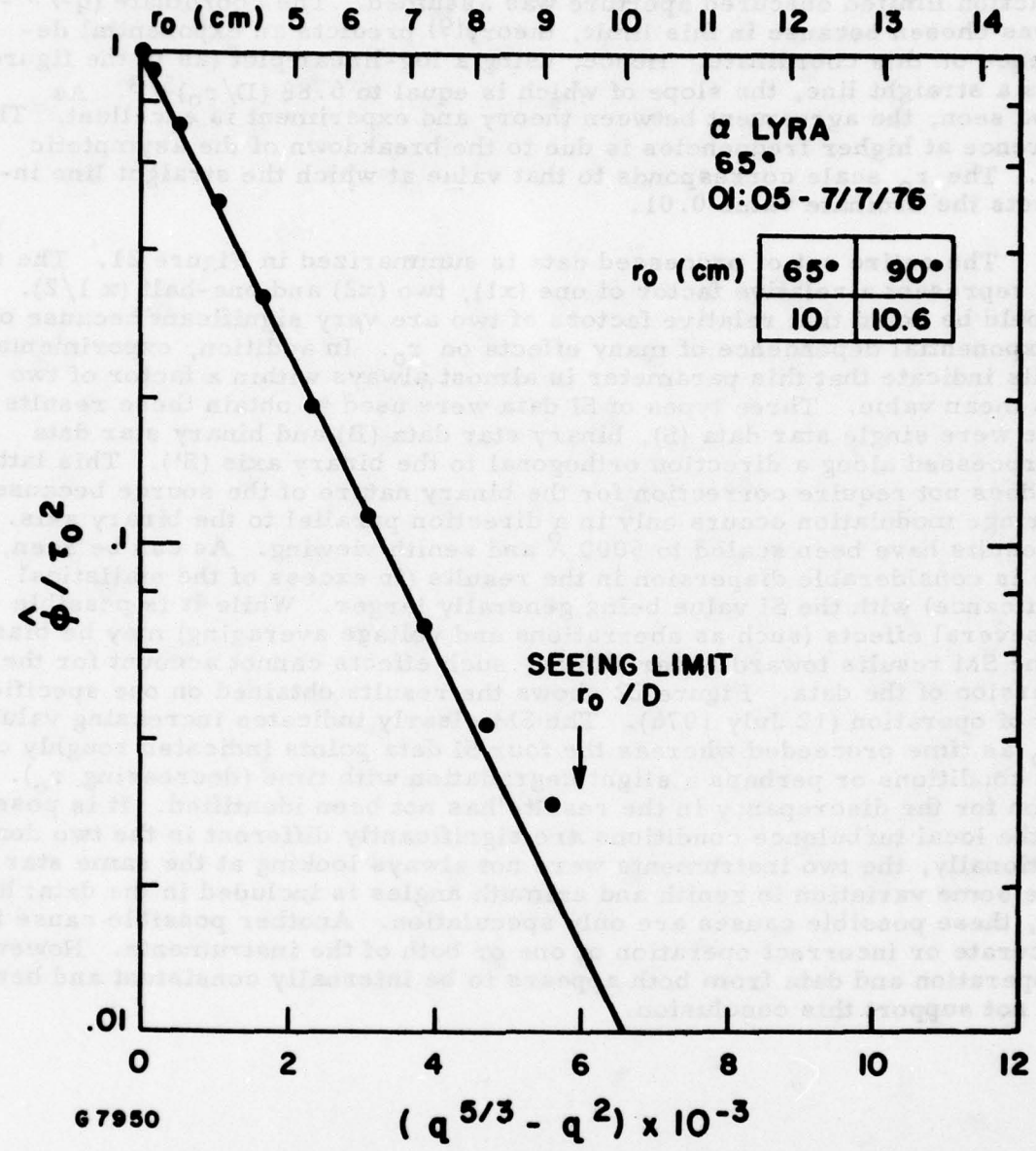

Figure 20 Determination of r_o from Speckle Data

diffraction limit of the telescope. For the purposes of evaluating r_o, a diffraction limited obscured aperture was assumed. The coordinate $(q^{5/3} - q^2)$ was chosen because in this limit, theory(9) predicts an exponential dependence on this coordinate. Hence, using a log-linear plot (as in the figure) yields a straight line, the slope of which is equal to $6.88\ (D/r_o)^{5/3}$. As can be seen, the agreement between theory and experiment is excellent. The difference at higher frequencies is due to the breakdown of the asymptotic form. The r_o scale corresponds to that value at which the straight line intersects the ordinate value 0.01.

The entire set of processed data is summarized in Figure 21. The solid lines represent a relative factor of one (x1), two (x2) and one-half (x 1/2). It should be noted that relative factors of two are very significant because of the exponential dependence of many effects on r_o. In addition, experimental results indicate that this parameter is almost always within a factor of two of its mean value. Three types of SI data were used to obtain these results. These were single star data (S), binary star data (B) and binary star data but processed along a direction orthogonal to the binary axis (S'). This latter data does not require correction for the binary nature of the source because the fringe modulation occurs only in a direction parallel to the binary axis. All results have been scaled to 5000 Å and zenith viewing. As can be seen, there is considerable dispersion in the results (in excess of the statistical significance) with the SI value being generally larger. While it is possible that several effects (such as aberrations and voltage averaging) may be biasing the SM results toward lower values, such effects cannot account for the dispersion of the data. Figure 22 shows the results obtained on one specific night of operation (12 July 1976). The SM clearly indicates increasing values of r_o as time proceeded whereas the four SI data points indicates roughly constant conditions or perhaps a slight degradation with time (decreasing r_o). A reason for the discrepancy in the results has not been identified. It is possible that the local turbulence conditions are significantly different in the two domes. Additionally, the two instruments were not always looking at the same star and hence some variation in zenith and azimuth angles is included in the data; however, these possible causes are only speculation. Another possible cause is inaccurate or incorrect operation of one or both of the instruments. However, the operation and data from both appears to be internally consistent and hence does not support this conclusion.

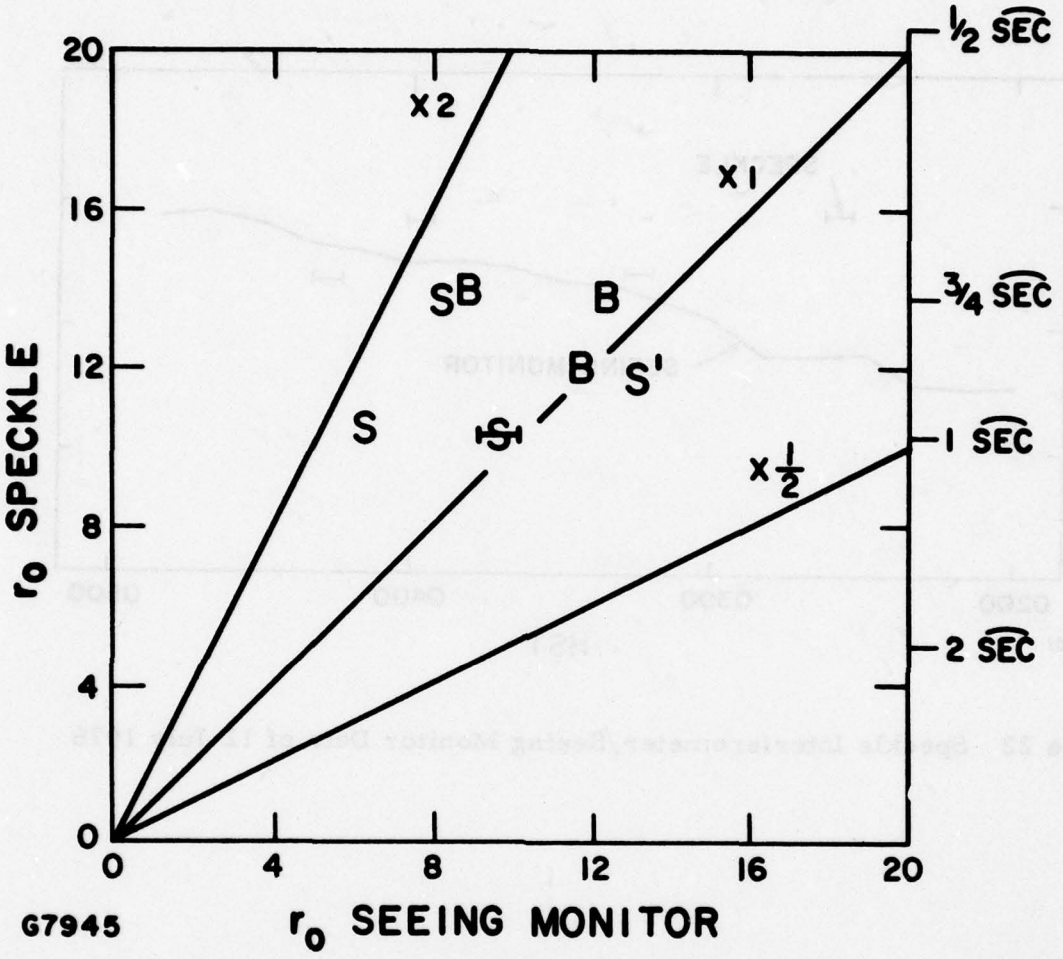

Figure 21 Speckle Interferometer/Seeing Monitor Comparison

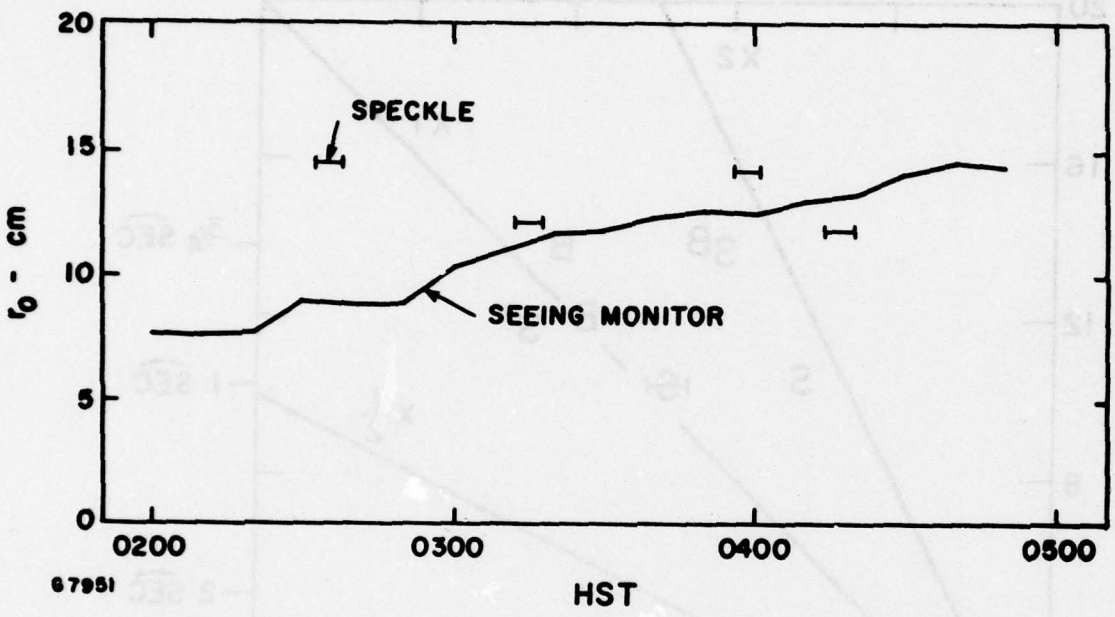

Figure 22 Speckle Interferometer/Seeing Monitor Data of 12 July 1976

3.3 STAR SENSOR DATA AND ANALYSIS

3.3.1 Statistical Properties of Profile Data

A variety of statistical properties of the profile data[3] collected during the period 11 November 1975 to 13 July 1976 have been determined. Table 3 gives the mean, variance and standard deviation to mean ratio for the one hundred and twenty-six member ensemble of C_n^2 values at each of the seven nominal altitudes. These results are presented graphically in Figure 23. The three solid lines represent the mean, mean plus one standard deviation and the maximum values of C_n^2 obtained. The broken line is the Hufnagel averaged wind correlated model[11] with an upper atmospheric wind speed of 12.5 m/s. This value is somewhat lower than would be expected based on the analysis of a limited amount of meteorological data (20-30 m/s seems to be more typical). Higher values in the model would yield a larger tropopause bump which is not indicated by the data. While such increases of turbulence levels are indicated on some occasions, the average profile shows only a flattening in the vicinity of the meteorological tropopause.

Figure 24 is the cumulative probability distribution for the entire seven level ensemble of empirical C_n^2 values. In order to present all of the data on a single plot, the values at each altitude were normalized by dividing by the average value of C_n^2 at that altitude. The natural logarithm of the normalized data was then used to generate the CPD. The solid line represents a Gaussian distribution (log-Gaussian for C_n^2) with the empirical mean and variance. These results should be compared with the parameter r (h, t) in the Hufnagel model which is assumed to be a Gaussian random variable with zero mean and a variance of two. The data has a mean of approximately 0.5 and a variance of 1.2. The non-zero empirical mean is probably due to the finite and non-zero threshold of the Star Sensor. The output below this threshold is dominated by noise and in some cases negative values result. Obviously, negative and zero values must be eliminated in the subsequent processing. The result of suppressing small values of C_n^2 would be to bias the mean towards a positive value. The variance of r (h, t) assumes, of course, point averaging in time (t) and altitude (h). Hufnagel's model includes the altitude and time covariance function which has two characteristic time scales (5 and 80 minutes) and two characteristic altitude scales (100 and 2,000 meters). The instrument bases its estimate of C_n^2 on data collected over a twenty minute time period and the theoretical weighting functions used in the processing are of variable width. However, all are considerably wider than 100 meters; hence, an empirical variance of less than two is to be expected.

---

(11) R. E. Hufnagel, Variations of Atmospheric Turbulence, OSA Topical Meeting on Optical Propagation Through Turbulence (Boulder, Colorado, July 1974). Paper WA1.

TABLE 3. STATISTICAL PARAMETERS OF AVERAGE PROFILE

Nominal Altitude Above Site (km)	C_n^2 Mean ($\times 10^{-18} m^{-2/3}$)	C_n^2 Variance ($\times 10^{-36} m^{-4/3}$)	SD/M
2.25	17.1	336.6	1.07
3.75	9.0	92.6	1.07
5.25	4.7	49.0	1.49
7.5	4.3	26.6	1.20
9.75	3.6	16.2	1.12
12.75	2.4	6.4	1.05
>14.5	1.2	1.6	1.05

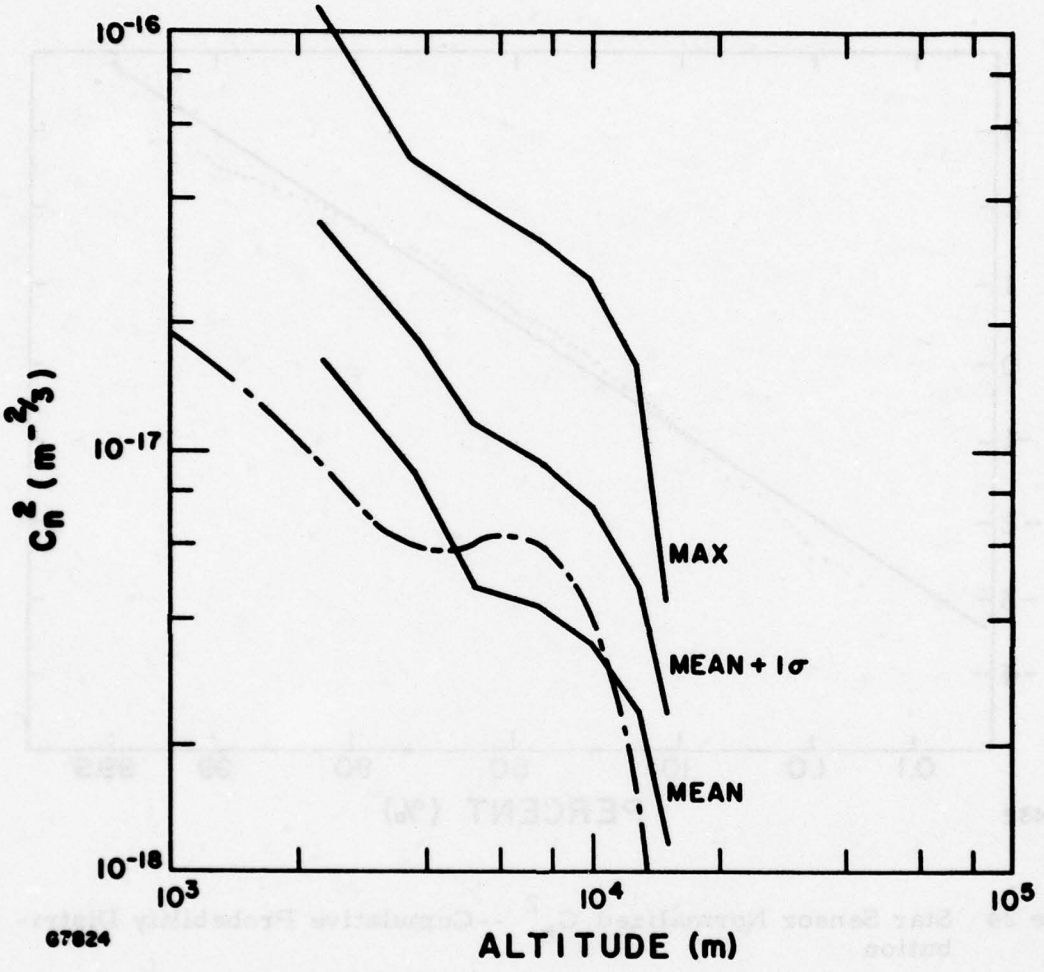

Figure 23 Star Sensor Average Profile

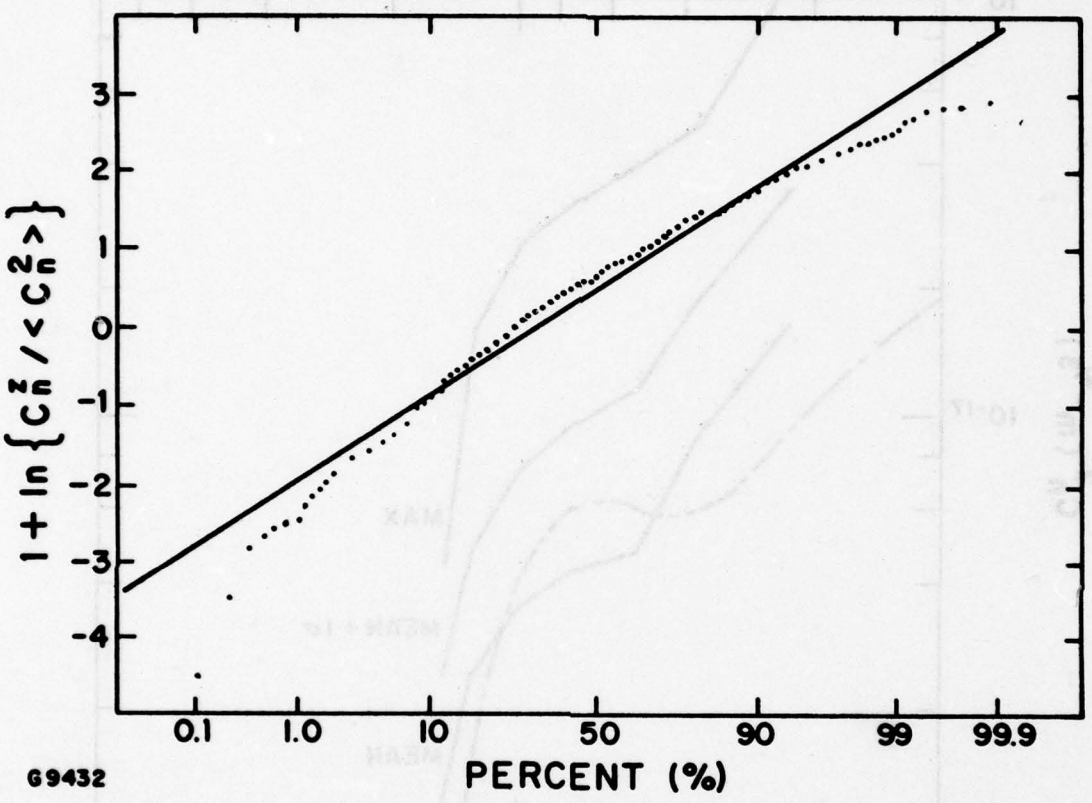

Figure 24 Star Sensor Normalized C_n^2 --Cumulative Probability Distribution

3.3.2 Routine Data

During this period data was collected with the Star Sensor on eight occasions. The results are summarized in Table 4. The yield, defined as the number of profiles collected with scintillation standard deviation to mean ratios of 0.2 or less compared to the total number of complete profiles collected, averaged 62.5%. This is quite close to previous experience[3] and continues to indicate that significant atmosphere non-stationarity over twenty minute periods occurs approximately 40% of the time.

The nightly averaged profiles are given in Figures 25 and 26. Only two of the profiles (29 October and 13 January) indicated significant increases in turbulence levels which are consistent with the existence of a tropopause bump. Four others (22-24 September, 27 October and 12 January) only show a flattening of the curve at higher altitudes which appears to be the typical behavior of the upper atmosphere above AMOS. Two of the profiles are of rather unusual shape. On 28 October the profile shows rather strong turbulence (3×10^{-17} $m^{-2/3}$) at 2.25 kM which decreases slowly at first and then more rapidly at high altitudes. Essentially no turbulent activity is indicate about 14.5 kM. While unusual, this type of behavior has been observed on at least one other occasion (18 June 1976) inwhich the profile was very similar in shape but yielded stronger turbulence (by approximately a factor of two) at all levels but the highest. The profile of 10 December is also unusual and not at all consistent with the various models. The 2.25 kM value is the lowest ($\simeq 4 \times 10^{-19}$ $m^{-2/3}$) observed for any nightly average data collected to date. However, the very high levels in the (5-10) kM range have been observed on at least three other occasions. The unique aspect in this case is that turbulence levels increased by approximately a factor of forty within an altitude range of less than 3 kM and then remained virtually constant for more than 5 kM of altitude.

The average profile (based on 34 samples) for the entire period is given in Table 5. These results should be compared with the averages for the previous period given in Table 3. Comparing the two results, it can be seen that somewhat higher average values (10-60%) exist at all levels in the present case; however, the non-existence of a tropopause bump continues to be indicated. Also included in Table 5 is the average profile for the entire data base that presently exist (160 profiles taken over the period 15 October 1975 to 15 March 1977). This profile is within 3-13% of that shown in Figure 23. The only change in the maximum value profile is at the highest level. In one profile collected during this period a value of 10^{-17} $m^{-2/3}$ was observed in the greater than 14.5 kM range. This is approximately a factor of two greater than that value shown in Figure 23.

Sixty samples of the aperture averaged twenty minute log-amplitude variance were collected during the period. They ranged from $(1.8 - 14.1) \times 10^{-4}$ with a mean value of 5.88×10^{-4}. This data is very consistent with the previous measurements,[3] the means agreeing to within 1%.

TABLE 4. STAR SENSOR DATA SUMMARY

Date	Time HST	Yield	No. of Samples	σ_1^2 ($\times 10^{-4}$) Range	Mean
22 Sept 1976	0100-0300	3/6	6	1.78 - 2.30	2.17
24 Sept 1976	0050-0520	3/6	7	1.48 - 3.05	2.14
27 Oct 1976	2000-0100	7/9	10	3.93 - 9.80	5.61
28 Oct 1976	2030-2320	3/5	5	4.64 - 8.14	5.91
29 Oct 1976	1840-2250	5/5	6	5.00 - 9.94	7.09
10 Dec 1976	1900-2230	3/7	8	5.21 - 13.16	9.08
12 Jan 1977	1950-2230	5/8	8	4.41 - 11.96	8.07
13 Jan 1977	1930-2240	5/10	10	2.03 - 14.12	5.92

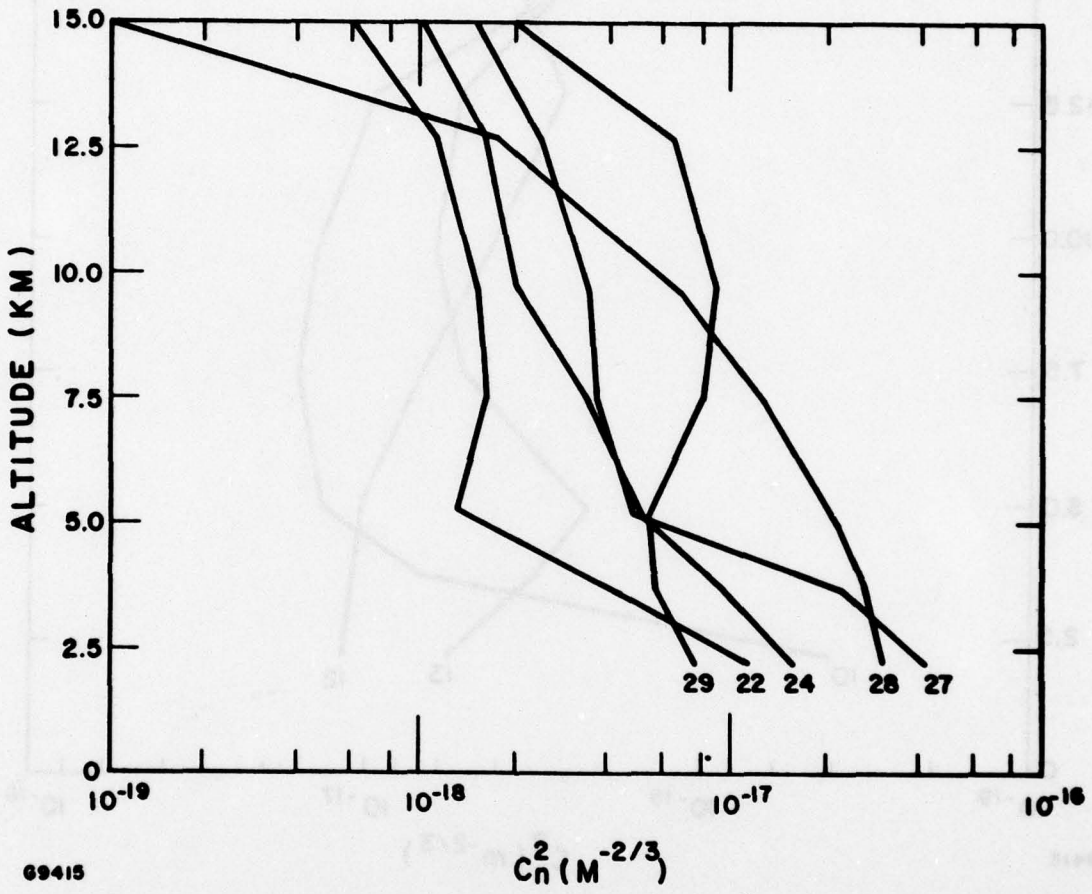

Figure 25 Star Sensor Nightly Averaged Profiles for 22 and 24 September and 27, 28 and 29 October 1976. Altitude is in height above the observatory. Each profile is an average of all valid data collected on a specific night. The widths of the weighting functions are not shown.

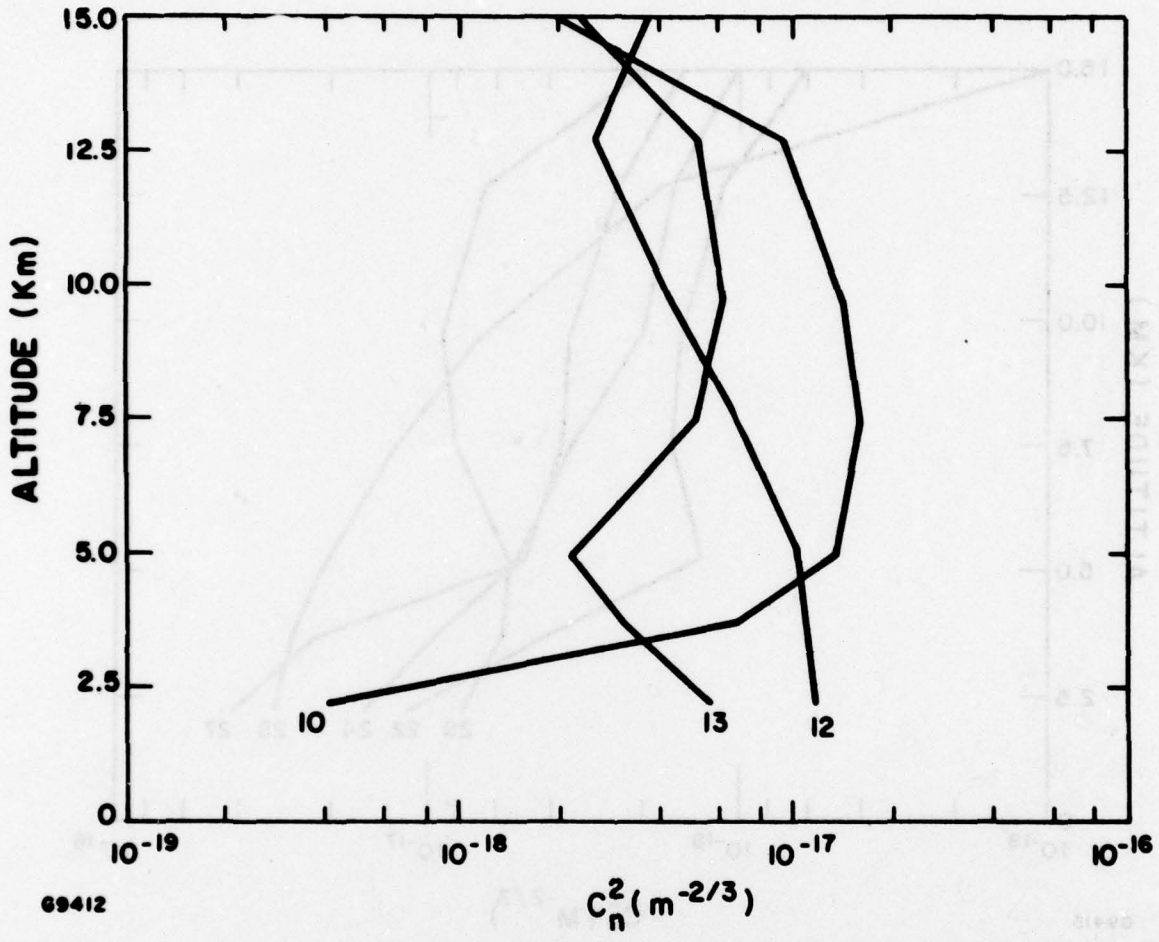

Figure 26 Star Sensor Nightly Averaged Profile for 10 December 1976 and 12 and 13 January 1977 (Same as Figure 25)

TABLE 5. AVERAGE PROFILES

Normal Altitude Above Site (km)	C_n^2 ($\times 10^{-18} m^{-2/3}$) 15 Sept 1976 - 15 Mar 1977	C_n^2 ($\times 10^{-18} m^{-2/3}$) 15 Oct 1975 - 15 Mar 1977
2.25	19.6	17.6
3.75	11.9	9.6
5.25	7.4	5.3
7.5	6.7	4.8
9.25	5.7	4.0
12.75	3.9	2.7
>14.5	1.8	1.3

3.4 RTAM DATA

Initial AMOS operations with the modified RTAM occurred during the period 24-28 January 1977. The objective of these tests was to evaluate field performance and document the results via the collection of five photographs of oscilloscope traces for five different stars (25 photographs in total). The required data for each star consists of four MTF traces (minimum and maximum electrical bandwidth at two different time scales) and one PTF trace. The data was collected on 28 January 1977 and is shown in Figures 27 to 31. The MTF traces (four upper pictures) have a vertical scale of 1 volt/division and horizontal scales of 500 μsec/division and 50 μsec/division for the left and right hand pictures, respectively. The upper and lower MTF's are for minimum and maximum bandwidth, respectively. The bottom picture is a dual trace of the MTF and phase with a 2 volt/division vertical scale and a 50 μsec/division horizontal scale. Also included in the figures are the star name, magnitude and elevation angle.

For these tests, the RTAM was mounted on the 1.6 m telescope. No external spectral filtering was used and only a small amount of light was split-off for the boresight camera. The instrument was optimized for single channel operation. Observing conditions were not good due to intermittent high clouds. Operations had to be suspended for approximately two hours due to total cloud cover.

As can be seen from the figures, the performance is similar to that observed previously.[3] The central peak (low spatial frequencies) of seeing limited size is clearly defined; however, the noise dominated pedestal (at high spatial frequencies) is somewhat higher due to a modification of the electronics. The phase signals are now in a different format with a spatial frequency scaling identical to the MTF (i.e., $-|f|$ to the left, zero at the center and $+|f|$ to the right). Modification of the electronics also allows the phase to lock back onto the correct value after dropout due to insufficient MTF signal if the MTF rises above threshold; however, the essential conclusion reached previously still remains. Because of insufficient sensitivity, it is unlikely that either the MTF or phase can be successfully processed for high spatial frequency information. At low frequencies, the width of the peak can be used to estimate r_o. The data reported here indicates a value in the range of (5-7) cm. This is only a rough estimate and while low, is not inconsistent with previous experience.

A considerable improvement in the field of view has been effected. For single channel operation, it is now approximately ± 4 arc seconds in both directions.

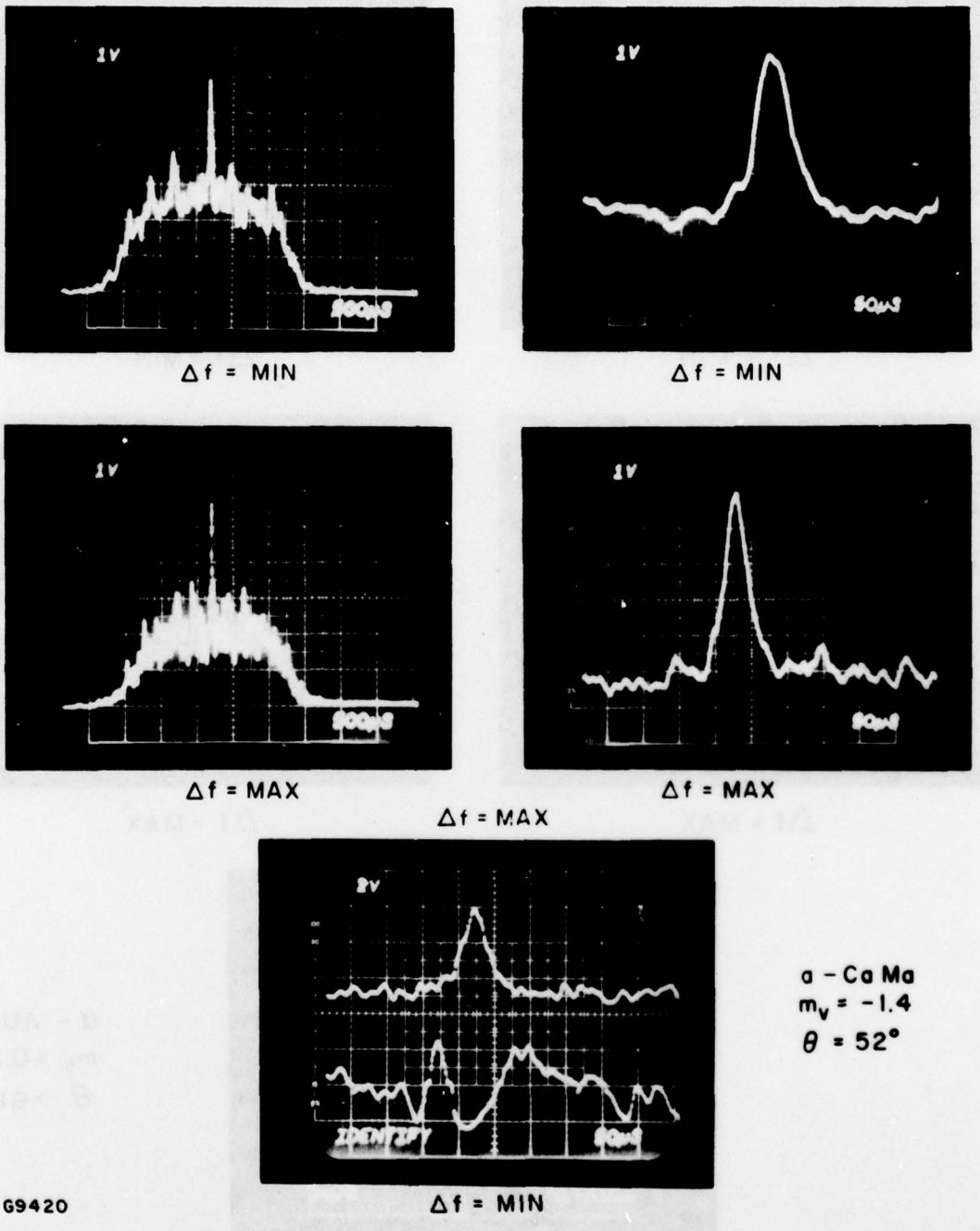

Figure 27 RTAM Data. The object is α-CaMa (m = -1.4). The upper four photographs are MTF traces at minimum (upper) and maximum (lower) electronic bandwidth. The lower photograph is a dual trace of the MTF and PTF.

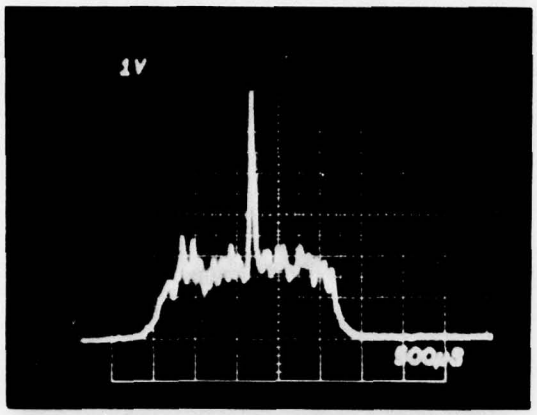

Δf = MIN

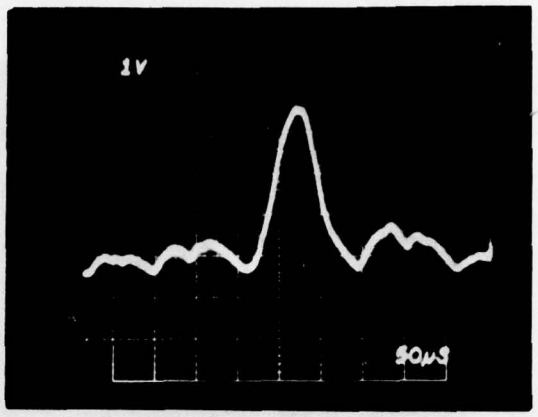

Δf = MIN

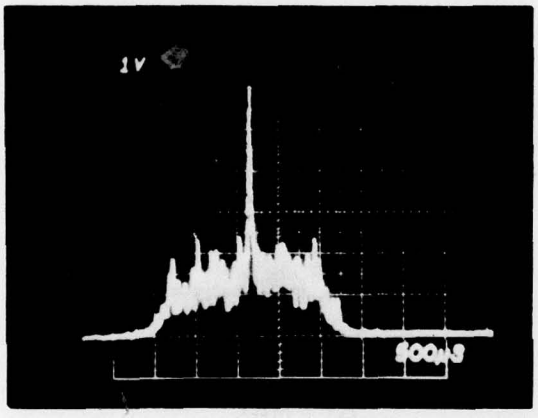

Δf = MAX

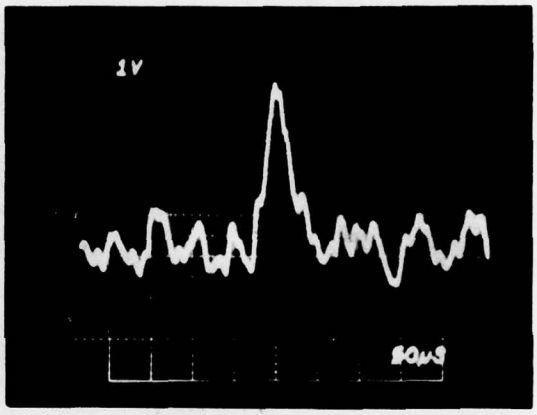

Δf = MAX

Δf = MAX

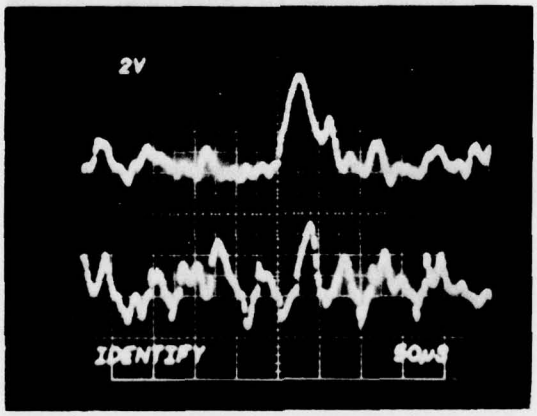

α - AUR
m_v = 0.2
θ = 61°

G9406

Δf = MAX

Figure 28 RTAM Data. The object is α-Ori (m = 0.0)--(same as Figure 27)

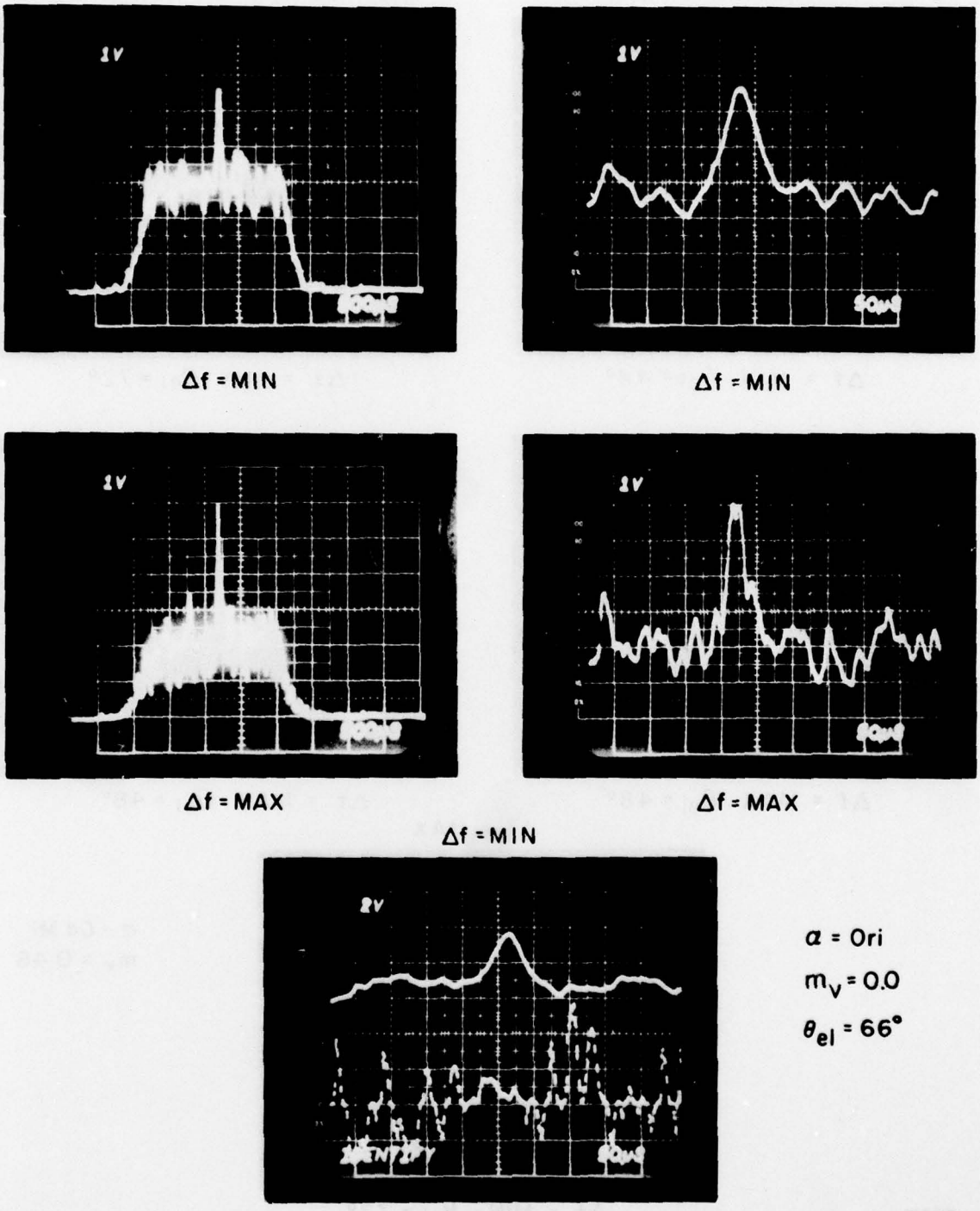

Figure 29 RTAM Data. The object is α-Aur (m = 0.2)--(same as Figure 27)

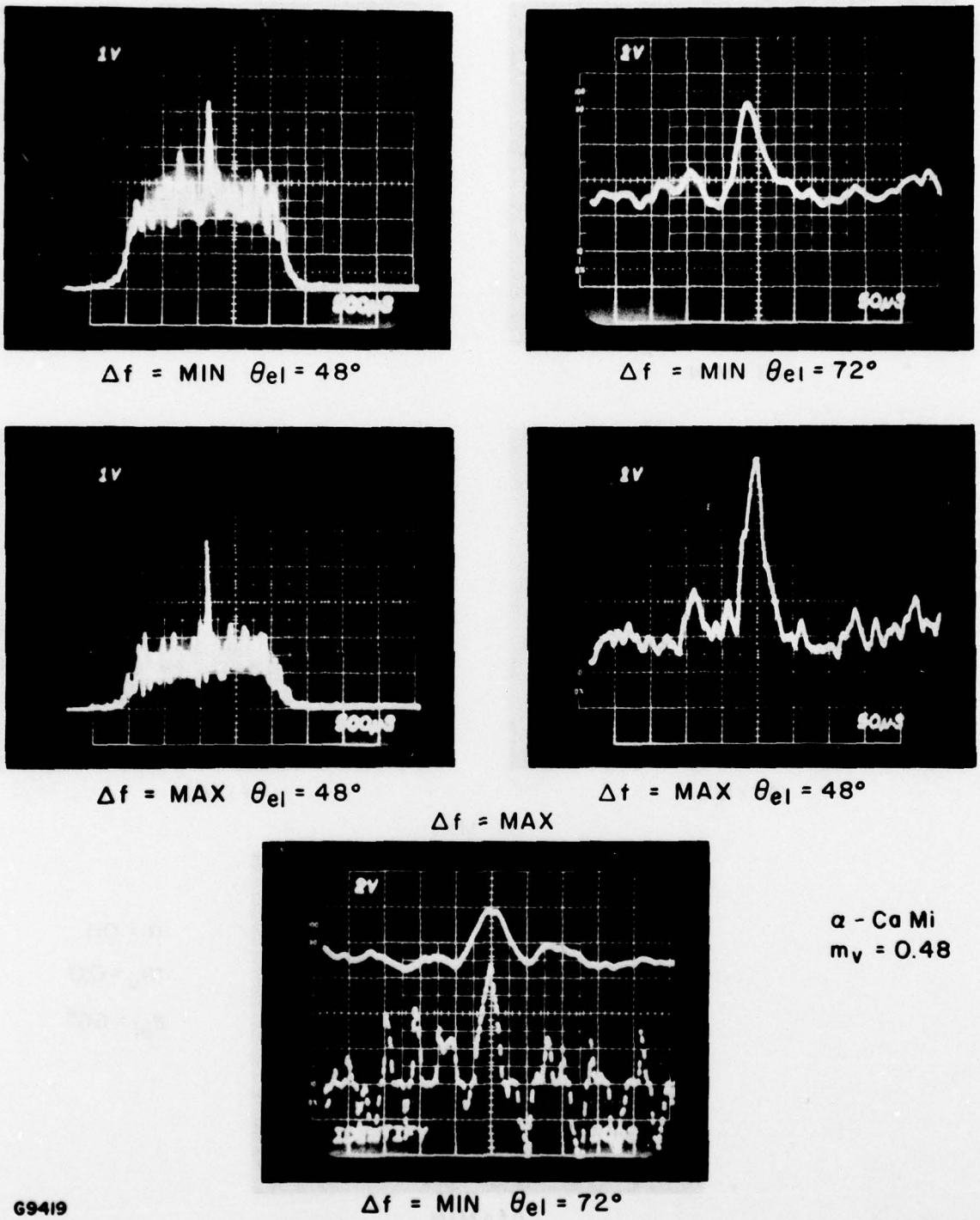

Figure 30 RTAM Data. The object is α-CaMi (m = 0.48)--(same as Figure 27)

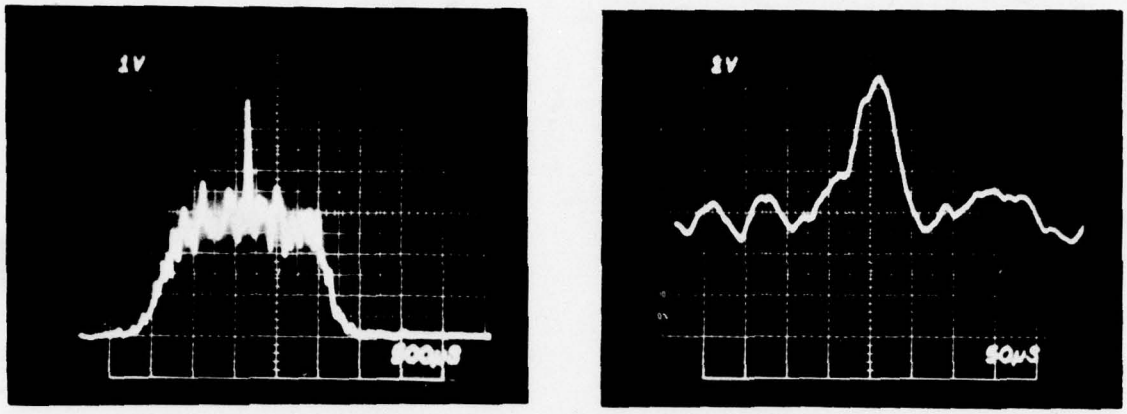

Δf = MIN θ_{el} = 86°

Δf = MIN θ_{el} = 86°

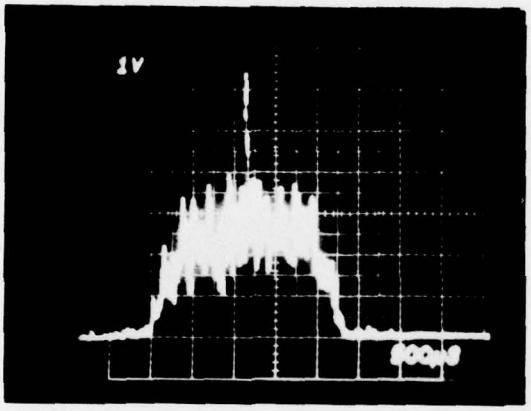

Δf = MAX θ_{el} = 86°

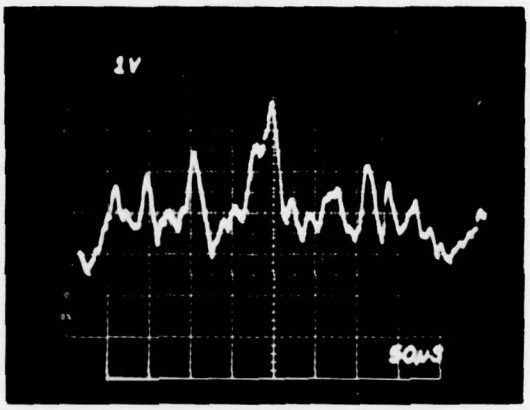

Δf = MAX θ_{el} = 86°

Δf = MIN

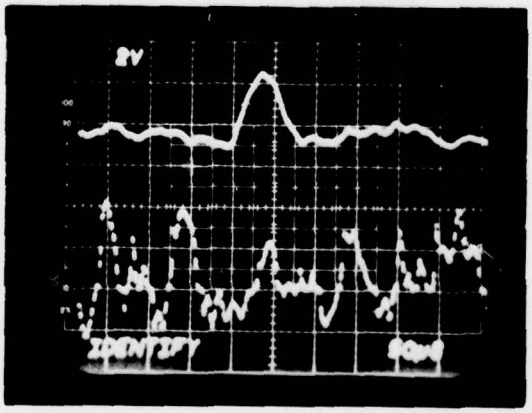

α - Tau

m_v = 1.06

G9407

Δf = MIN θ_{el} = 53°

Figure 31 RTAM Data. The object is α-Tau (m = 1.06)--(same as Figure 27)

REFERENCES

1. M. G. Miller and P. F. Kellen, Turbulence Characterization and Control, Interim Technical Report, Contract F30602-75-C-0012 (Avco Everett Research Laboratory, Inc.), Rome Air Development Center Technical Report #RADC-TR-75-185 (July 1975), (A015759).

2. M. G. Miller, P. L. Zieske and G. Dryden, Turbulence Characterization and Control, Final Technical Report, Contract F30602-75-C-0012 (Avco Everett Research Laboratory, Inc.), Rome Air Development Center Technical Report #RADC-TR-76-189 (June 1976), (A027155).

3. M. G. Miller and P. L. Zieske, Turbulence Environment Characterization, Interim Technical Report, Contract F30602-76-C-0054 (Avco Everett Research Laboratory, Inc.), Rome Air Development Center Technical Report #RADC-TR-77-70 (March 1977).

4. D. P. Greenwood, D. O. Tarazano, D. A. Haugen, J. C. Kaimal, J. Newman, P. F. Kellen and M. G. Miller, AMOS Seeing Quality Measurements, Rome Air Development Center Technical Report #RADC-TR-75-295 (January 1976), (A021943).

5. J. C. Wyngarrd, J. Izumi and S. A. Collins, Jr., Behavior of the Refractive-Index--Structure Parameter Near the Ground, J. Opt. Soc. Am. 61, 1646 (1971).

6. G R. Giuliano, J. A. Jenney, L. Miller, M. E. Pedinoff, D. Y. Tseng and S. M. Wandzura, Space Object Imaging, Final Technical Report, Contract F30602-74-C-0227 (Hughes Research Laboratories), Rome Air Development Center Technical Report #RADC-TR-76-54 (March 1976), (A023497).

7. J. C. Dainty, Stellar Speckle Interferometry, in Laser Speckle and Related Phenomena, Topics in Applied Physics Vol. 9, Ed. by J. C. Dainty (Springer-Verlag, Berlin, 1975).

8. A. M. Schneiderman and D. P. Karo, How to Build a Speckle Interferometer, Proc. of SPIE, 75, 70 (1976).

9. D. Korff, Analysis of a Method for Obtaining Near Diffraction Limited Information in the Presence of Atmosphere Turbulence, J. Opt. Soc. Am. 63, 971 (1973).

10. D. L. Fried, Optical Resolution Through a Randomly Inhomogeneous Medium for Very Long and Very Short Exposures, J. Opt. Soc. Am. 56, 1372 (1966).

11. R.E. Hufnagel, Variations of Atmospheric Turbulence, OSA Topical Meeting on Optical Propagation Through Turbulence (Boulder, Colorado, July 1974). Paper WA1.

MISSION
of
Rome Air Development Center

RADC plans and conducts research, exploratory and advanced development programs in command, control, and communications (C^3) activities, and in the C^3 areas of information sciences and intelligence. The principal technical mission areas are communications, electromagnetic guidance and control, surveillance of ground and aerospace objects, intelligence data collection and handling, information system technology, ionospheric propagation, solid state sciences, microwave physics and electronic reliability, maintainability and compatibility.